

UNCLASSIFIED

AD 419082

DEFENSE DOCUMENTATION CENTER

FOR

SCIENTIFIC AND TECHNICAL INFORMATION

CAMERON STATION, ALEXANDRIA, VIRGINIA



UNCLASSIFIED

NOTICE: When government or other drawings, specifications or other data are used for any purpose other than in connection with a definitely related government procurement operation, the U. S. Government thereby incurs no responsibility, nor any obligation whatsoever; and the fact that the Government may have formulated, furnished, or in any way supplied the said drawings, specifications, or other data is not to be regarded by implication or otherwise as in any manner licensing the holder or any other person or corporation, or conveying any rights or permission to manufacture, use or sell any patented invention that may in any way be related thereto.

64-5

CATALOGED BY DDC 419082

AS AD NO.



DEPARTMENT OF METEOROLOGY
THE UNIVERSITY OF WISCONSIN
MADISON, WISCONSIN.

*EMPIRICAL AND THEORETICAL
STUDIES OF
ATMOSPHERIC ENERGETICS*

CONTRIBUTIONS BY:

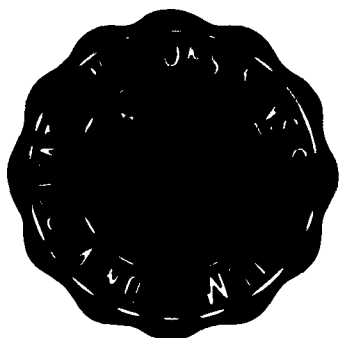
- E. G. ASTLING J. A. DUTTON
- R. A. BRYSON D. R. JOHNSON
- R. J. DELAND W. SCHWERTFEGER
- L. H. HORN, PRINCIPAL INVESTIGATOR

ANNUAL REPORT

THE RESEARCH REPORTED IN THIS DOCUMENT
HAS BEEN SUPPORTED BY THE UNITED STATES
WEATHER BUREAU UNDER CONTRACT CWB 10240.

15 SEPTEMBER 1962

419082



DEPARTMENT OF METEOROLOGY
THE UNIVERSITY OF WISCONSIN
MADISON, WISCONSIN.

*EMPIRICAL AND THEORETICAL
STUDIES OF
ATMOSPHERIC ENERGETICS*

CONTRIBUTIONS BY:

E. G. ASTLING J. A. DUTTON
R. A. BRYSON D. R. JOHNSON
R. J. DELAND W. SCHWERTFEGER
L. H. HORN, PRINCIPAL INVESTIGATOR

ANNUAL REPORT

THE RESEARCH REPORTED IN THIS DOCUMENT
HAS BEEN SUPPORTED BY THE UNITED STATES
WEATHER BUREAU UNDER CONTRACT CWB 10240.

15 SEPTEMBER 1962

TABLE OF CONTENTS

	<u>Page</u>
I. Introduction	iii
II. An Analysis of the Geostrophic Kinetic Energy Spectrum of Large-Scale Atmospheric Turbulence. By Lyle H. Horn and Reid A. Bryson.	1
III. A. On the Maintenance of the Southern Circumpolar Vortex (General Remarks). By W. Schwerdtfeger	17
B. The Southern Circumpolar Vortex and the Spring Warming of the Polar Stratosphere. By W. Schwerdtfeger.	19
IV. The Relation between Atmospheric Entropy and Available Potential Energy. By John A. Dutton	45
V. A Study of Terrestrial Radiation Measured by TIROS II. By Elford G. Astling and Lyle H. Horn	70
VI. A Study of the Movement of Long Atmospheric Waves. By R. J. Deland	100

INTRODUCTION

Differential heating of the atmosphere by the sun has been long recognized as the source of the kinetic energy of the atmosphere. However, the mechanisms through which the differential heating produces and maintains the kinetic energy of various scales of atmospheric circulation remains as one of the most challenging problems of meteorology. The research presented here, in the form of an annual report, consists of five papers representing various approaches to this basic problem. They have been prepared by a University of Wisconsin research group with support of United States Weather Bureau Contract CWB 10240.

To adequately meet the problem posed above, a number of complex atmospheric processes must be considered. The scales of atmospheric heating and cooling must be described — not only seasonal variations, but also such variations as those that occur between land and sea or between cloud-covered and clear areas. The generation of available potential energy which may be produced by the differential heating requires description, as does the conversion of the available potential energy to the kinetic energy of various scales of atmospheric circulation. The transfer of kinetic energy from one scale of circulation to another and the nature of its eventual dissipation are also pertinent.

Although during the past decade numerous efforts have been directed to this complex problem, an adequate solution is not at hand. However, the ever growing supply of observational data, conventional as well as that provided by earth satellites, is building a foundation upon which fruitful research may be based. The studies reported here represent some initial approaches by this research group to certain aspects of the problem.

The research reported by Astling and Horn represents an attempt to describe some of the gross aspects of the global heat budget using infrared radiation data supplied by the TIROS II satellite. Variations of terrestrial radiation between the winter and summer hemispheres, as well as differences between land and ocean areas, are described. As additional satellite data become available, more detailed studies of the heating and cooling processes of the atmosphere should be feasible. Such data, combined with radiation data measured by balloon-borne radiometers within the atmosphere, should provide significant information concerning the generation of available potential energy.

The article by Schwerdtfeger is a study of the largest scale of atmospheric kinetic energy — the southern hemisphere polar vortex. Because the surface features of the southern hemisphere are much more symmetrical than those of the northern hemisphere, the use of latitudinal means (of heights, thickness, and radiation patterns) seems to be justified for a first analysis of the gross features of the southern

vortex. The study reveals the role of the differential heating of the atmosphere in producing semi-annual maxima of the vortex. Additional studies concerning the stability of the vortex are planned. Eventually they will be extended to include the more complex northern hemisphere vortex.

The analysis by Horn and Bryson of the spectrum of large-scale atmospheric turbulence reveals a partitioning of the spectrum which may be of significance in the production and transfer of kinetic energy from one scale to another. Further studies making use of this partitioning may provide improved descriptions of the scale size at which atmospheric kinetic energy is produced and transferred to other scales of circulation.

The empirical study by Deland of the wave speeds associated with various wave numbers represents another attempt to describe the nature of large-scale atmospheric turbulence. His results indicate that the empirically measured wave speeds for wave numbers between 5 and 10 agree remarkably well with the speeds predicted by the Rossby wave speed formula. These wave numbers are also the same as those which fall within one portion of the partitioned spectrum which is described in this report by Horn and Bryson.

In the article by Dutton an alternate method of obtaining an expression for the available potential energy of the atmosphere is presented. Dutton also relates the concept of available potential energy to the

Second Law of Thermodynamics by showing that the expressions derived by Lorenz are consistent with the atmospheric entropy concepts presented by Lettau. However, additional theoretical developments of expressions of the available potential energy of the atmosphere are needed. For example, empirical studies require an expression for the available potential energy for a limited area rather than for the entire globe.

The order in which the individual articles appear in this report is not intended to suggest a systematic approach to the basic problem of describing the mechanisms through which the kinetic energy of the atmosphere is maintained. The articles represent studies of various aspects of the basic problem and have been printed in the order in which they were completed.

The preparation of the research reported here has involved a number of people not listed as authors of the individual articles. Mr. Donald Johnson has spent many hours in aiding in the preparation of the various articles and in editing this final report. Mr. Jack Hayter has assisted in the drafting of the figures and in the mechanics of the final preparation of the report.

Lyle H. Horn
Principal Investigator

Madison, Wisconsin
September 15, 1962

AN ANALYSIS OF THE GEOSTROPHIC KINETIC ENERGY SPECTRUM
OF LARGE-SCALE ATMOSPHERIC TURBULENCE

Lyle H. Horn
and
Reid A. Bryson

Abstract. The mean geostrophic kinetic energy spectrums of the large-scale atmospheric circulation features are presented for a six-month winter period for three elevations at three latitudes. The mean spectrums are partitioned into two sections, and a $8/3$ power relationship is noted between geostrophic kinetic energy and wavelength for the higher wave numbers. The physical significance of the partitioning and of the $8/3$ relationship is considered by comparing these results with the results obtained from other investigations of atmospheric energy processes. Certain comparisons indicate that the wavelengths described by the $8/3$ power relationship are those for which the two-dimensional turbulence is isotropic. Other comparisons suggest that these same wavelengths are those at which the kinetic energy of the atmosphere is produced.

Introduction. To study the scale size of atmospheric energy processes, several investigators have described the kinetic energy as a function of wave number around selected parallels of latitude. The reader is referred to Saltzman and Fleisher [1962] for a complete bibliography of such studies. In this paper the mean spectrums of geostrophic kinetic energy of the large-scale circulation features are presented for the 300-, 500-, and 700-mb isobaric surfaces at latitudes 25, 45, and 65° N for the period October 1, 1951, through March 31, 1952. The partitioning of kinetic energy between the various wave numbers is then further analyzed and the results compared with those obtained from other energy studies.

Procedures and basic data. The kinetic energy per unit mass is

$$K = (u^2 + v^2)/2 \quad (1)$$

where u and v are the eastward and northward wind components, respectively. In view of Parseval's theorem, the kinetic energy per unit mass averaged around a latitude circle may be expressed as

$$\frac{1}{2\pi} \int_0^{2\pi} K d\lambda = [\hat{u}^2(0) + \hat{v}^2(0)]/2 + \sum_{n=1}^{\infty} [\hat{u}^2(n) + \hat{v}^2(n)]/4 \quad (2)$$

where λ is longitude, $\hat{u}(0)$ and $\hat{v}(0)$ are the mean values of u and v , and $\hat{u}(n)$ and $\hat{v}(n)$ are the Fourier coefficients of the n th harmonic of the u and v components around a parallel of latitude. Thus

$\hat{u}^2(n)$ and $\hat{v}^2(n)$ are given by

$$\hat{u}^2(n) = \left[\frac{1}{\pi} \int_0^{2\pi} u(\lambda) \cos n\lambda d\lambda \right]^2 + \left[\frac{1}{\pi} \int_0^{2\pi} u(\lambda) \sin n\lambda d\lambda \right]^2 \quad (3)$$

$$\hat{v}^2(n) = \left[\frac{1}{\pi} \int_0^{2\pi} v(\lambda) \cos n\lambda d\lambda \right]^2 + \left[\frac{1}{\pi} \int_0^{2\pi} v(\lambda) \sin n\lambda d\lambda \right]^2 \quad (4)$$

Thus the eddy kinetic energy per unit mass contributed by the n th harmonic is

$$K(n) = [\hat{u}^2(n) + \hat{v}^2(n)]/4 \quad (5)$$

The reader is referred to Saltzman [1957] or Van Mieghem et al. [1959] for a detailed description of the Fourier method applied to the kinetic energy spectrum. In this study the mean spectrums were calculated geostrophically from the daily height values of the 300-, 500-, and 700-mb isobaric surfaces around three parallels of latitude, 25°, 45°, and 65°N.

The basic data consisted of daily values of the following:

- (1) Eastward and northward geostrophic wind components at 300 mb
[Lahey et al., 1960]
- (2) Heights of the 500 mb isobaric surface [Lahey et al., 1958]
- (3) Heights of the 700 mb isobaric surface (furnished by the Extended Forecast Section of the United States Weather Bureau).

All data points were spaced at 10° longitude intervals along parallels of latitude. Daily values of the geostrophic kinetic energy per unit mass for wave numbers 1 through 12 were computed. The daily values for each wave number were then averaged to obtain the mean spectrums for the six-month period.

Discussion of results. The mean spectrums of geostrophic kinetic energy per unit mass for the period October 1, 1951, through March 31, 1952, are presented in Figure 1. As expected, the largest spectral values occur at 300 mb, with progressively smaller values at 500- and 700-mb. Likewise, the relatively low energy levels at 25°N could be expected. At all latitudes the major portion of the geostrophic kinetic energy is found at low wave numbers (i. e., at longer wavelengths). The tendency for maximums at wave numbers 1 and 3 has been noted by Saltzman [1958] and Van Mieghem et al. [1959].

Figure 1 also reveals that beyond a certain lower n value there is a continuous decrease of kinetic energy with increasing wave number. Figure 2, which presents the graph of geostrophic kinetic energy per unit mass versus wavelength on logarithmic scales, permits a description of this decrease as a power law relationship. Wavelength rather than wave number has been chosen as the abscissa because the wavelength for a given wave number varies in proportion to the cosine of the latitude; however, the wave numbers are also indicated on Figure 2.

A striking feature revealed by this figure is a pronounced tendency to a linear distribution for the higher wave numbers. The feature is noted at all latitudes and isobaric surfaces considered. In each diagram a line of best fit has been drawn which can be expressed as

$$\log K = M \log L + \log c \quad (6)$$

where M is the slope of the line, L is wavelength, and c is an

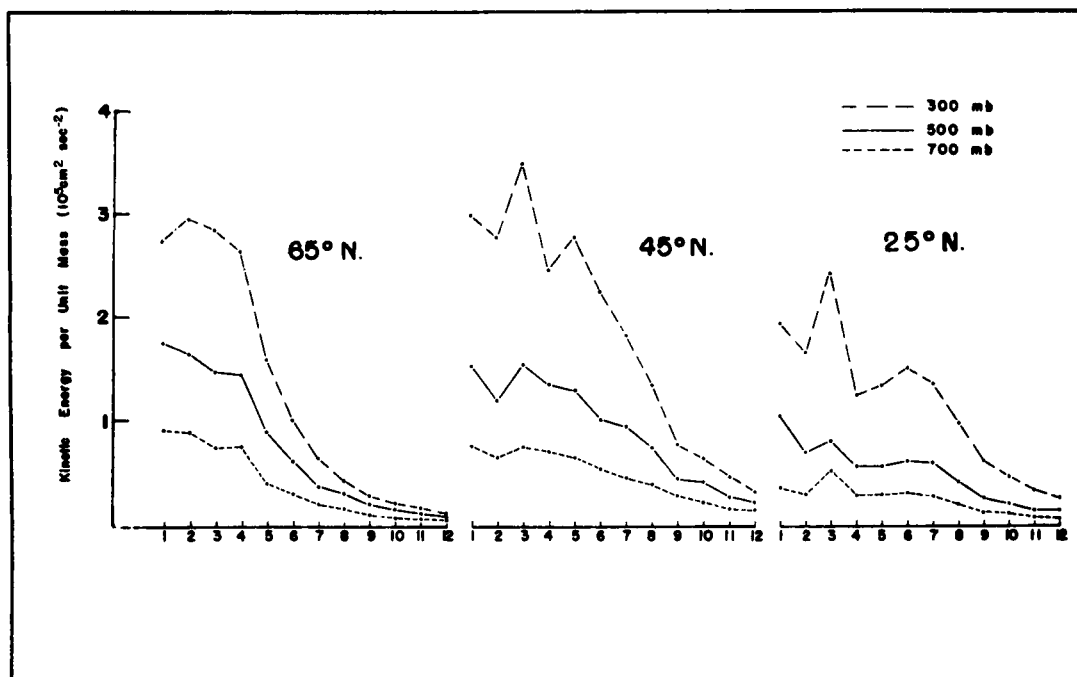


Figure 1. Mean spectra of geostrophic kinetic energy per unit mass at latitudes 65°N, 45°N, and 25°N for the period October 1, 1951, through March 31, 1952

arbitrary constant. Equation 6 is equivalent to a power law relationship between kinetic energy and wavelength,

$$K = cL^M \quad (7)$$

The slopes of the lines of best fit are indicated on each diagram of Figure 2. The \underline{M} values range from 2.9 to 2.3, with an average value of slightly less than $8/3$. Thus, for wavelengths shorter than approximately 5000 km, the geostrophic kinetic energy per unit mass is approximately proportional to the $8/3$ power of the wavelength. To objectively establish the range of wavelengths for which the $8/3$ power applies, another line of best fit (i. e. the dashed line) has been drawn for lower wave numbers. The intersection point of the two lines determines a special wavelength which has been indicated on each diagram of Figure 2. For example, at 300 mb at 65°N , the $8/3$ power relationship holds for wavelengths less than about 4300 km. The maximum value of wavelength for which the relationship applies appears to be relatively independent of pressure but does show a definite increase with decreasing latitude. At 65°N the intersections occur at 4200 to 4500 km, while at 25°N they occur at 5100 to 5200 km. Since the spectrums extend to only wave number 12, no attempt can be made to describe a minimum wavelength for which the $8/3$ power relationship applies. The lines for low wave numbers are supported only by relatively few and scattered points. An attempt to estimate the slope led to \underline{M} values ranging from 0.04 to 0.17, with an average of about 0.10.

The lines of best fit clearly partition the kinetic energy spectrum into two portions, one described by the $8/3$ power relationship, and one by a $1/10$ power relationship. The wavelengths which are independent of the $8/3$ relationship describe the circulation features which tend to be more persistent and of climatic significance. These large-scale features are usually considered the result of the distribution of oceans, continents, and mountain ranges. The wavelengths which fit the $8/3$ power are those associated with the atmosphere's more transient circulation features — its traveling cyclones and anticyclones.

Using somewhat different approaches, other investigators have also noted a tendency for the kinetic energy spectrum to be divided into two sections. White and Cooley [1956] studied frequency distributions for wave numbers associated with meridional circulations at 45°N and found a bimodal distribution with maximums at wave numbers 4 and 8. These maximums fall within the two groups of wave numbers discussed above. Van Mieghem et al. [1959] noted that at 50°N the principal portion of the kinetic energy of long waves ($n < 5$) is associated with quasi-stationary waves. On the other hand, he noted that the kinetic energy of moving waves tends to be more evenly distributed over all wave numbers. More recently, Saltzman and Fleisher [1962] found that more than 85 per cent of the kinetic energy associated with stationary circulation features occurs at long waves ($n = 1$ to 5); however, they note that not all long waves are stationary. These results seem to indicate that the kinetic energy spectrum consists of two rather distinct portions.

They also raise questions concerning the physical significance of the partitioning.

The partitioning portrayed by Figure 2 suggests a comparison with the partitioning of the kinetic energy spectrum of small-scale atmospheric turbulence (i. e. , of the order of 10^0 to 10^{-4} km). In the inertial subrange of small-scale isotropic turbulence, a $-5/3$ power relationship describes the distribution of kinetic energy for a range of wave numbers at which kinetic energy is transferred from larger to smaller eddies without production or dissipation of energy [MacCready, 1962]. Ogura and Miyakoda [1954] found that within this same range of wave numbers a $-7/3$ power relationship exists between pressure fluctuations and wave number. Returning to the case of large-scale turbulence, it is interesting to note that Syono et al. [1955] found that a $-7/3$ power relationship approximates the distribution of the mean-square amplitudes of a Fourier series ($n > 4$) of the heights of the 500-mb surface. A spectrum of the mean-square height amplitudes is essentially a spectrum of the kinetic energy of the meridional component of the geostrophic wind (i. e. , the pressure fluctuations around a parallel of latitude determine the geostrophic wind). Ogura [1958] has studied the spectrums of the 300-mb meridional (v) and zonal (u) geostrophic kinetic energy and their product (uv), and has discussed the $-7/3$ power relationship in large-scale atmospheric turbulence. He notes that for the wave numbers included by the $-7/3$ power relationship the spectrum of uv is an order of magnitude less than the spectrums of

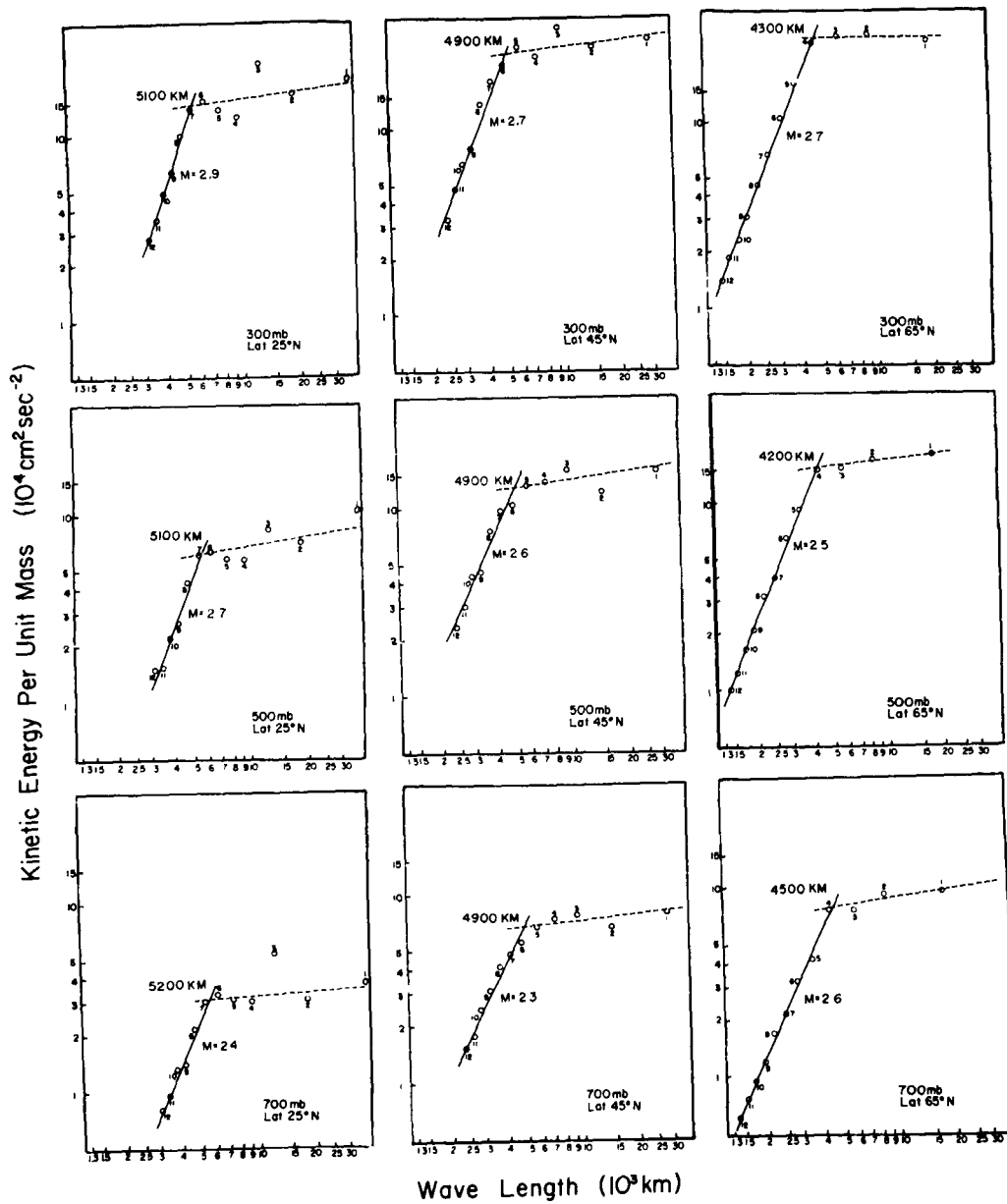


Figure 2. Mean spectrums of the log of geostrophic kinetic energy per unit mass versus the log of wavelength for the period October 1, 1951, through March 31, 1952. Small numbers next to data points indicate wave numbers. Other notation is described in the text.

either u^2 or v^2 , indicating that within this range of wave numbers the two-dimensional large-scale turbulence tends to be isotropic.

Using wave number rather than wavelength as the abscissa of Figure 2, a $-8/3$ power relationship between kinetic energy and wave number is obtained. This value agrees tolerably well with the $-7/3$ power relationship mentioned above. Although the mean slope of the lines on Figure 2 is about $8/3$, the slopes tend to steepen with decreasing pressure. The average slope for the three latitudes increases from 2.43 at 700 mb to 2.60 at 500 mb to 2.77 at 300 mb. The increasing slope reflects the tendency for the amplitudes of the shorter wavelengths to become damped with height. Ogura [1958], who has worked with data for only one pressure level, has predicted that a multiple level analysis would reveal such an increase of slope with height.

It is instructive to further examine the Figure 2 data in light of Ogura's results. Ogura found that for the spectral values which lie along a straight line, the two-dimensional large-scale turbulence at latitudes 20° and 70°N shows strong evidence of being isotropic, while at intermediate latitudes the turbulence shows less evidence of isotropy. Figure 2 provides supporting evidence. At 25° and 65°N the spectral values for the higher wave numbers show a remarkable tendency to fall along a straight line; however, at 45°N a deviation is noted — especially for wave numbers 6 to 9. This departure might be considered as evidence of a larger horizontal momentum transfer (uv)

at 45°N [Lahey et al., 1960]. In general, Ogura's results appear to indicate that the partitioning of the kinetic energy spectrum revealed by Figure 2 may be interpreted as a division between isotropic and anisotropic turbulence.

Recent empirical studies concerning the conversion of available potential energy to kinetic energy as a function of wave number provide an additional comparison with the results obtained here. Saltzman and Fleisher [1960b, 1961] found that the greatest conversion of available potential energy to kinetic energy occurs at wave number 6. Wiin-Nielsen [1959] has found a maximum conversion at wave numbers 6 and 7, but has also noted a secondary maximum at wave numbers 2 and 3. Saltzman and Fleisher [1960a] have noted that there is a net transfer of kinetic energy from the range of wave numbers 6 to 10 to both higher and lower wave numbers, indicating that a net conversion of available potential energy occurs at wave numbers 6 to 10. It is noteworthy that the scale of these circulation features coincides with the scale of the features described by the $8/3$ power relationship.

Since the above studies indicate that scale features the size of atmospheric disturbances (i. e., cyclones and anticyclones) may be the principal mechanisms for the conversion of available potential energy to kinetic energy, it is of interest to compare the Figure 2 data with the predictions of baroclinic instability theory. In an atmosphere possessing a sufficient degree of baroclinity, theory predicts that a certain range of wavelengths will amplify and that the wavelength corresponding to

maximum amplification will increase with decreasing latitude [Eliassen, 1956]. The range of wavelengths described by the $8/3$ power relationship falls within the range predicted by the theory. Furthermore, the upper limit of the wavelength (i. e. , the line intersections on Figure 2) increases from 4200 to 4500 km at 65°N to 5100 to 5200 km at 25°N .

Summary. The results obtained in this study indicate that the spectrum of the kinetic energy of large-scale turbulence is partitioned into two distinct portions, one described by an $8/3$ power law and one independent of it. Comparisons with other energy studies suggest that the partitioning is physically significant. A comparison with Ogura's results indicates that the $8/3$ relationship describes a portion of the spectrum for which the two-dimensional turbulence is isotropic, while the turbulence which is independent of the $8/3$ power is anisotropic. This characteristic is most evident at 25° and 65°N . On the other hand, comparisons with the results of Saltzman and Fleisher [1960a, 1960b] and Wiin-Nielsen [1959] and baroclinic instability theory suggest that the wavelengths included in the $8/3$ relationship represent the portion of the spectrum at which the principal conversion of available potential energy to kinetic energy occurs.

The data used in this study consist of a relatively small sample. Likewise, the studies with which it has been compared were, for the most part, based on as small or smaller data samples. Nevertheless, the results attained suggest the desirability of further investigation into

the partitioning of the kinetic energy spectrum.

Acknowledgments. The research reported in this paper has been supported by the United States Weather Bureau under contract Cwb-10240.

We wish to thank Professors Heinz Lettau and Raymond Deland, Dr. John Dutton, and Mr. Donald Johnson for their assistance in various portions of the study.

REFERENCES

- Eliassen, A. , Instability theories of cyclone formation, in Weather Analysis and Forecasting, vol. I, by S. Petterssen, McGraw-Hill Book Co. , New York, pp. 313-319, 1956.
- Lahey, J. F. , et al. , Atlas of 500 mb Wind Characteristics for the Northern Hemisphere, University of Wisconsin Press, Madison, 1958.
- Lahey, J. F. , et al. , Atlas of 300 mb Wind Characteristics for the Northern Hemisphere, University of Wisconsin Press, Madison, 1960.
- MacCready, P. B. , The inertial subrange of atmospheric turbulence, J. Geophys. Research, 67, 1051-1059, 1962.
- Ogura, Y. , On the isotropy of large-scale disturbances in the upper troposphere, J. Meteorol., 15, 375-382, 1958.
- Ogura, Y. , and K. Miyakuda, Note on pressure fluctuations in isotropic turbulence, J. Meteorol. Soc. Japan, 32, 160-166, 1954.
- Saltzman, B. , Equations governing the energetics of the larger scales of atmospheric turbulence in the domain of wave number, J. Meteorol., 14, 513-523, 1957.

Saltzman, B., Some hemispheric spectral statistics, J. Meteorol., 15, 259-263, 1958.

Saltzman, B., and A. Fleisher, The exchange of kinetic energy between larger scales of atmospheric motion, Tellus, 12, 374-377, 1960 a.

Saltzman, B., and A. Fleisher, The modes of release of available potential energy in the atmosphere, J. Geophys. Research, 65, 1215-1222, 1960 b.

Saltzman, B., and A. Fleisher, Further studies on the modes of release of available potential energy, J. Geophys. Research, 66, 2271-2273, 1961.

Saltzman, B., and A. Fleisher, Spectral statistics of the wind at 500 mb, J. Atmospheric Sciences, 19, 195-204, 1962.

Syono, S., A. Kasahara, and Y. Sekiguti, Some statistical properties of the atmospheric disturbances on the 500 mb level, J. Meteorol. Soc. Japan, 33, 23-30, 1955.

Van Mieghem, J., P. Defrise, and J. Van Isacker, On the selective role of the motion systems in the atmospheric general circulation, in The Atmosphere and Sea in Motion, edited by B. Bolin, Rockefeller Institute Press, New York, pp. 230-239, 1959.

White, R. , and D. Cooley, Kinetic energy spectrum of meridional motion in the mid-troposphere, J. Meteorol., 13, 67-69, 1956.

Wiin-Nielsen, A. , A study of energy conversion and meridional circulation for the large-scale motion in the atmosphere, Monthly Weather Rev., 87, 319-332, 1959.

ON THE MAINTENANCE OF THE
SOUTHERN CIRCUMPOLAR VORTEX

W. Schwerdtfeger

General Remarks. The troposphere throughout the year and the stratosphere during the major part of the year are colder in the polar regions than in middle latitudes. This state of the atmosphere is the result of radiation processes and the vertical transport of heat, both of which generally tend to increase the meridional temperature gradient. On the other hand, macroscale horizontal exchange processes tend to decrease it. The interaction of these processes produce northern and southern hemisphere circumpolar vortices, their seasonal variations and their shorter term disturbances.

Only in the southern hemisphere however, may we expect to find a mean vortex (monthly or seasonal) which is approximately circular and pole-centered. In the northern hemisphere, the distribution of continents and oceans disturbs the symmetry of the radiation processes

and other mechanisms of heat transfer, causing a more complex atmospheric thickness field and circulation pattern.

Because of the approximate symmetry of the southern hemisphere vortex, a diagnostic study of the interaction of the various dynamic processes can lead to interesting conclusions, even though only limited aerological data are available. One of the pertinent topics is the maintenance of the southern circumpolar vortex by the production of available potential energy through differential meridional heating and its conversion into kinetic energy.

The following study is intended as an analysis of only one particular feature of the southern westerlies, the equinoctial maxima of the intensity of the circumpolar vortex. This feature is related to another characteristic of the southern vortex, which is the late and relatively regular appearance of the "breakdown" of the stratospheric vortex and the accompanying weakening of the tropospheric circulation. In future studies the energy processes and the associated problem of the stability of pole-symmetric and asymmetric vortices will be examined.

THE SOUTHERN CIRCUMPOLAR VORTEX AND THE
SPRING WARMING OF THE POLAR STRATOSPHERE*

W. Schwerdtfeger

Abstract. The yearly march of the meridional temperature differences between middle and polar latitudes of the southern hemisphere shows a predominance of the annual component at the surface and in the stratosphere, and of the semi-annual in the troposphere. An examination of the various terms in the heat budget of the troposphere leads to the conclusion that the absorption of incoming solar radiation is the only term which has meridional differences with a stronger semi-annual than annual variation, and with the proper phase. An estimate of the efficiency of this type of differential heating indicates that its magnitude is large enough to account for the observed yearly march of the meridional tropospheric temperature gradient. This semi-annual periodicity also contributes to the seasonal change of the strength of the

*A paper presented at the International Symposium on Stratospheric and Mesospheric Circulation, Berlin, August 1962.

stratospheric circumpolar vortex which attains its maximum, at least up to the 50 mb level, in September. The differential heating by absorption of solar radiation is thus considered the forcing factor which tends to re-establish the pole-centered vortex after cyclonic developments in the strong circumpolar westerlies have disturbed its nearly circular symmetric features. Only after the September peak does the efficiency of this process decrease significantly.

A. Introduction

In comparison to the data available for a study of the northern polar vortex, the aerological evidence needed to describe the behavior of the southern vortex is still rather incomplete. Nevertheless, various analyses for the troposphere (Rastorguev and Alvarez, 1958; Alt, Astapenko and Ropar, 1959; Van Loon, 1961; the microfilms of the Antarctic Analysis Center Melbourne, 1960 and 1961) and for the stratosphere (Palmer and Taylor, 1959; Moreland, 1960; Farkas, 1961) indicate that during the winter and the first weeks of spring the southern vortex differs from its northern counterpart in two respects: 1) its nearly circular symmetric form with the center not far from the Pole, and 2) the fact that a major "breakdown" of the vortex appears well after the spring equinox.

In the following the relationship between these two phenomena is discussed and the principal cause of the observed characteristics of the southern vortex is considered. Since the stratospheric circulation is definitely coupled to the tropospheric circulation, the proposed approach must start from a consideration of the tropospheric conditions. Such an approach should make evident how the surface and tropospheric conditions of the southern hemisphere determine the different behavior of the southern vortex.

The seasonal variation of the amount of solar energy incoming at different latitudes, due to the geometry of the sun-earth system, and

the resulting reactions of the atmosphere can be considered as a radiation experiment of major scale. Therefore, an analysis of the yearly march of certain meteorological parameters (i. e. , mean meridional temperature gradients, strength of the mean zonal winds, etc.) can provide insight into some of the atmospheric processes brought about by the changing energy input.

Seasonal variations should appear in the simplest form on a planet of uniform surface characteristics (i. e. , either all water, all ice, all land without mountains and also of uniform thermal properties and of uniform atmospheric moisture content). Such an atmosphere is generally called a planetary atmosphere, and its circulation, a planetary circulation. If we maintain the condition of uniform surface characteristics only with reference to longitude, admitting changes of surface parameters with latitude, we will use the term "quasi-planetary atmosphere."

In considering the possible seasonal variations of a quasi-planetary circulation, the effects of differential heating on the mean meridional temperature gradients in the troposphere and stratosphere are of principal concern. Thus an analysis of the yearly variation of the heat budget of the atmosphere at different latitudes and in the two principal layers is in order.

In this paper, however, attention will only be given to the question of determining whether there appear, in the differences (middle latitudes minus polar latitudes) of each term of the heat budget, any shorter

periodicities than the simple annual variation, and if so, for which term or terms. Such a question is relevant and can be used as a simple tool for a study of the possible causal relations; the reasoning is that an harmonic analysis of two finite series consisting of the 12 monthly values (defining the yearly march of any parameter) can show whether the amplitude of the n^{th} harmonic component of both series is zero or very small, thus indicating that the series produced by superposition of the two original series will also have a zero or very small n^{th} harmonic component.

B. Seasonal variations of the heat budget

We consider the following different terms of the heat budget of a quasi-planetary atmosphere:

1. Solar heating
2. Infrared cooling
3. Net latent heating
4. Heat flux from the underlying surface
5. Heat storage in the atmosphere.

Since we wish to study the seasonal variations of differential heating, we must examine the composition of the yearly march of the southern hemisphere latitudinal differences of each of these terms. The results of this examination will then be compared with a 5-year series of the mean meridional temperature gradients in the troposphere and in the lower stratosphere between 50 and 80° S. Values of the extraterrestrial radiation at these two latitudes and of certain atmospheric parameters at stations near these latitudes will be used where needed.

1. Terms 2, 3, and 5: Gabites (1960) has studied the heat balance for the southern hemisphere south of 40° S in order to assess the southward transport of heat necessary to maintain the observed state of the Antarctic atmosphere. From his computations of the mean monthly values of the various items of the atmospheric heat budget between 40 and 90° S we can deduce the following statements:

- a) The meridional differences ($50 - 80^{\circ}$ S) of the mean upward flux of long wave radiation (computed from Gabites' Fig. 3) show a simple annual variation, from high values in fall and winter to lower values in summer.
- b) The same holds true for the net latent heat term (Gabites' Fig. 7) but with smaller values for the yearly average and for the amplitude of the yearly variation.
- c) The meridional differences of the heat storage in the atmosphere are negative in the first half, positive in the second half of the year, and can be considered, on the whole, the least important item of the atmospheric heat budget.

Considering our insufficient knowledge of atmospheric parameters in the southern hemisphere, particularly of the moisture conditions in the free atmosphere, it can be said that the monthly values computed by Gabites are only first estimates which must be improved when more detailed and exact observational data become available. However, the only feature of major concern for the present study (i. e., the character of the seasonal variations) can be assessed sufficiently: the yearly

march of the meridional differences of the three terms of the heat budget considered here — items 2, 3, and 5 — each shows a simple annual variation. A semi-annual variation, if present at all, is definitely much smaller.

The other two items — heating by absorption of short wave radiation in the atmosphere, and heat flux from the surface — need special consideration. In Gabites' study, mean monthly values at different latitudes are given only for a term which he called effective solar radiation, comprising both the part absorbed in the atmosphere and at the surface. Although this combination was apparently suitable for the purpose of estimating the meridional heat transport, it will not be adequate for the purposes of this paper. Therefore, the solar heating term must be considered in more detailed form.

2. Solar heating: The meridional differences are represented in Fig. 1 (see also: Schwerdtfeger, 1960). The monthly means, in ly/day, of the incoming solar radiation (at the top of the atmosphere), computed from the well known values of Milankovitch, are the following:

Table 1. Monthly means of incoming solar radiation

Lat.	(ly/day)					
	I	II	III	IV	V	VI
50° S	1030	860	630	410	250	180
80° S	<u>1050</u>	<u>650</u>	<u>210</u>	<u>20</u>	<u>0</u>	<u>0</u>
Diff.	-20	210	<u>420</u>	390	250	180
Lat.	VII	VIII	IX	X	XI	XII
50° S	200	330	530	760	950	1070
80° S	<u>0</u>	<u>0</u>	<u>110</u>	<u>450</u>	<u>910</u>	<u>1140</u>
Diff.	200	330	<u>420</u>	310	40	-70

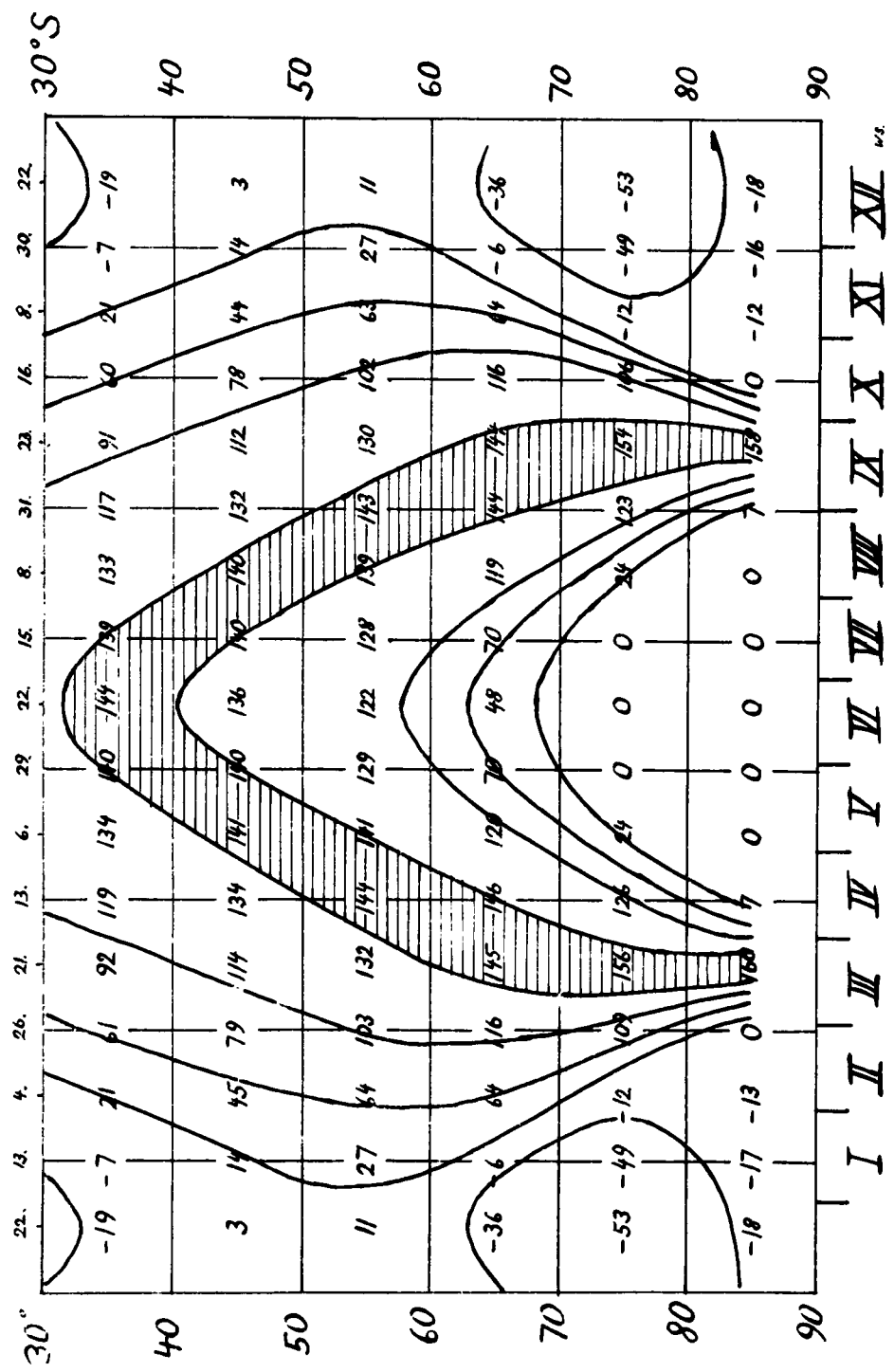


Figure 1. 10° latitude differences of daily totals (ly) of incoming solar radiation (at the top of the atmosphere) between 30° and 90° S, derived from Milankovitch.

The equinoctial maxima in the yearly march of the differences are quite conspicuous. Of course, immediately the question arises as to what portion of the total incoming energy can be absorbed in the atmosphere. For the troposphere, water vapor content and cloudiness are the decisive factors. Accordingly, aerological soundings at middle and polar latitudes of the Southern hemisphere have been used to determine approximate mean monthly values of the "liquid equivalent" (a concept adopted instead of "precipitable water," following the proposition by Myers, 1962) at 50 and 80° S.

Table 2. The mean liquid equivalent (cm) at 50 and 80° S

Lat.	<u>I</u>	<u>II</u>	<u>III</u>	<u>IV</u>	<u>V</u>	<u>VI</u>
50° S	1.5	1.5	1.4	1.3	1.1	1.0
80° S	.5	.5	.4	.3	.2	.2
Lat.	<u>VII</u>	<u>VIII</u>	<u>IX</u>	<u>X</u>	<u>XI</u>	<u>XII</u>
50° S	.9	.9	1.0	1.1	1.2	1.4
80° S	.15	.15	.15	.2	.3	.4

Even if these approximate values should be as much as 20% in error, which seems possible on the ground of the doubtful measurements of humidity at low temperatures, the effect on the following considerations would be negligible. The principal feature in both series is the simple yearly variation with the maximum late in summer and the minimum in late winter and early spring.

Using these values, Tables 6a-e of Korb et al. (1956) with their extension to 80° lat. can be used to obtain the monthly means of the

daily sums of the radiation absorbed in a vertical column of humid air without clouds between 1000 and 300 mb. Additionally, the absorption of solar radiation in clouds has to be taken into account. Here once more, values obtained by Möller and his collaborators (Korb et al., l. c, Table 8 and Fig. 20, Möller, 1960) may be used after certain assumptions are made as to cloud type, amount, and their vertical extent at 50 and 80° S during the course of the year. The extensive cloud coverage over the southern oceans throughout the year is well known, and on the knowledge of the frequency of strong cyclonic developments, considerable mean thickness of the cloud layer can be supposed to prevail. Over the Antarctic continent, there is on the average less cloudiness, particularly so in winter and spring, but this is of little consequence for our problem since there is no or very little incoming radiation at these latitudes at this time. As a first approximation the following mean monthly percentages of absorption of incoming short wave radiation by clouds may be acceptable.

Table 3. Absorption of incoming short wave radiation
in clouds (%)

Lat.	<u>I</u>	<u>II</u>	<u>III</u>	<u>IV</u>	<u>V</u>	<u>VI</u>	<u>VII</u>	<u>VIII</u>	<u>IX</u>	<u>X</u>	<u>XI</u>	<u>XII</u>
50° S	5	5	4	4	3	3	3	4	4	4	5	5
80° S	3	3	3	2	-	-	-	-	2	3	3	3

Although the amount of energy absorbed in the cloudless layer below a cloud layer is less than that computed for the corresponding part of a cloudless, humid atmosphere, this condition has not been accounted

for here. Its effect is considered small because of the frequency of low cloud bases. Furthermore, vague assumptions would be necessary if it were considered. Therefore, the following estimates of the amounts of incoming radiation absorbed in the troposphere at 50 and 80° S are more likely to be somewhat too high than too low. It is felt, nevertheless, that the computed values are good enough to describe the essential features of differential solar heating between 50 and 80° S.

Table 4. Monthly mean values of short wave radiation absorbed in the troposphere (ly/day)

Lat.	<u>I</u>	<u>II</u>	<u>III</u>	<u>IV</u>	<u>V</u>	<u>VI</u>
50° S	155	130	96	72	49	32
80° S	<u>111</u>	<u>64</u>	<u>28</u>	<u>5</u>	<u>0</u>	<u>0</u>
Diff.	44	66	68	67	49	32
Lat.	<u>VII</u>	<u>VIII</u>	<u>IX</u>	<u>X</u>	<u>XI</u>	<u>XII</u>
50° S	39	61	83	108	141	164
80° S	<u>0</u>	<u>0</u>	<u>14</u>	<u>43</u>	<u>88</u>	<u>131</u>
Diff.	39	61	69	65	53	33

These values show immediately that the differential heating between middle and polar latitudes, as far as absorption of incoming solar radiation is concerned, has a pronounced semi-annual variation with equinoctial maxima. Harmonic analysis of the yearly march gives the following values for the amplitude (r) and phase (ϕ) of the first (annual) and second (semi-annual) harmonic components and the ratio of the variance accounted for by the higher harmonics to the total variance (R):

$r_1 = 2 \text{ ly/day}$; $\varphi_1 = 77^\circ$; maximum at January 13.

$r_2 = 19 \text{ ly/day}$; $\varphi_2 = 288^\circ$; maxima at March and September 22.

$R = 0.04$.

On the ground of the possible inadequacies introduced by the simplifying assumptions for the absorption of short wave radiation in the troposphere, only the values of second harmonic amplitude and phase can be accepted as significant.

Some brief comments on the physical implications of these values may be in order: The annual mean of the analyzed series is 54 ly/day . Thus on the annual average, the air column between 1000 and 300 mb (about the entire troposphere) at 50° S absorbs 54 ly more every day than the troposphere at 80° S . However, near the time of the equinoxes it is about 68 ly , and at the time of the solstices about 32 ly . The absorption of 100 ly in the 1000 to 300 mb layer corresponds to a warming of 0.6° K . Thus, if solar heating were the only term in the heat budget of the troposphere, in March and September the increase of the mean temperature of the latitudinal belt at 50° S would amount to 0.4° K/day (12° K per month) more than the increase at 80° S . On the other hand, in June and December, it would be only 0.2° K/day (6° K per month). Of course, other terms in the heat budget of the troposphere, in particular infrared cooling (stronger in middle than in polar latitudes) and meridional mass exchange (Grossaustausch) contribute to the real temperature variations so that there is no increase of contrasts between different latitudes from year to year. However, if the meridional differences of

these other terms do not also present semi-annual variations of comparable amplitude and phase, the semi-annual variation caused by differential solar heating must show up in the meridional temperature gradients of the troposphere. This, as a matter of fact, it does.

Fig. 2 shows clearly that the semi-annual component is important in the mean yearly march of the meridional temperature differences computed for the five years April 1957 to March 1962. Fig. 3 presents, in the form of a harmonic dial, the result of a separate analysis of the five available 12-month series, in order to arrive at an estimate of the statistical significance of the mean curve.

As far as the absorption of solar radiation in the stratosphere is concerned, the conditions are quite different from those in the troposphere. There is much stronger heating mainly due to ozone during the polar summer, smaller seasonal variations at middle latitudes, and thus a pronounced first harmonic component in the yearly march of the differential heating ($50 - 80^{\circ} S$) and a smaller second harmonic, $r_2 < r_1$.

This will not be substantiated, at the moment, by detailed computations based on scanty observations, but reference can be made to MacDowall (1960), in particular his Figures 17 and 35, and to the fact that the above statement regarding stratospheric conditions is true even in the northern hemisphere, as can be derived from the studies of Davis (1961, Table III) and Ohring (1958, Fig. II).

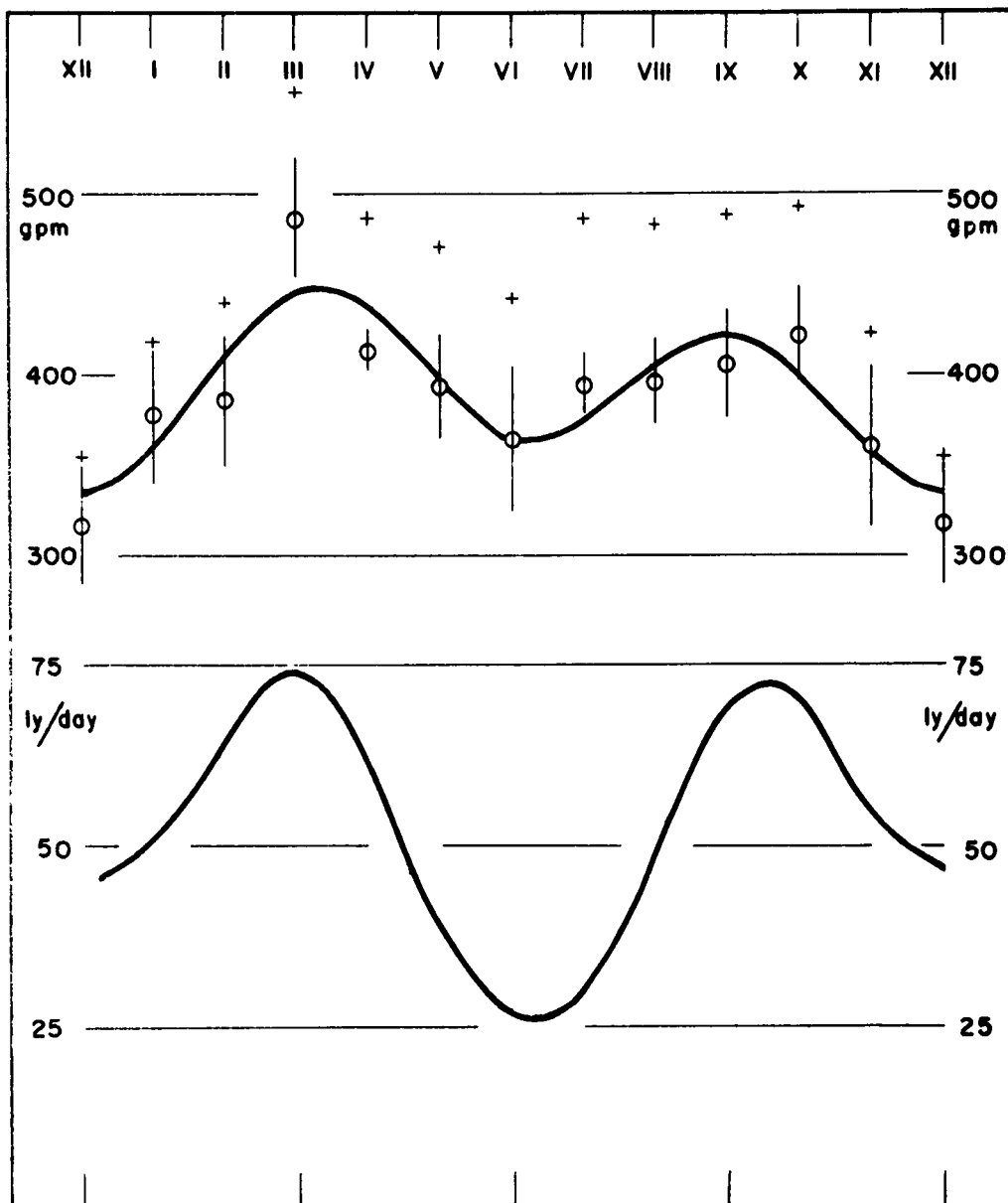


Figure 2. Yearly march of the mean meridional differences for the 300-700 mb thickness and for the computed values of solar radiation absorbed in the troposphere. a) Crosses: 5-year mean values of the thickness differences, (Port Stanley + Marion + Invercargill)/3 minus the South Pole (gpm). b) Circles: same as a) but reduced to differences for 50 minus 80° S (gpm). c) Vertical lines through the circles represent 2 standard deviations of each monthly mean difference (for $N = 5$, $\sigma_m = \sigma/\sqrt{5}$). d) Upper curve: sum of the first and second harmonic components of the yearly march of thickness differences (50 - 80° S). e) Lower curve: sum of the first and second harmonic components for the differences of short wave radiation absorbed in the troposphere (values from Table 4 for 50 minus 80° S).

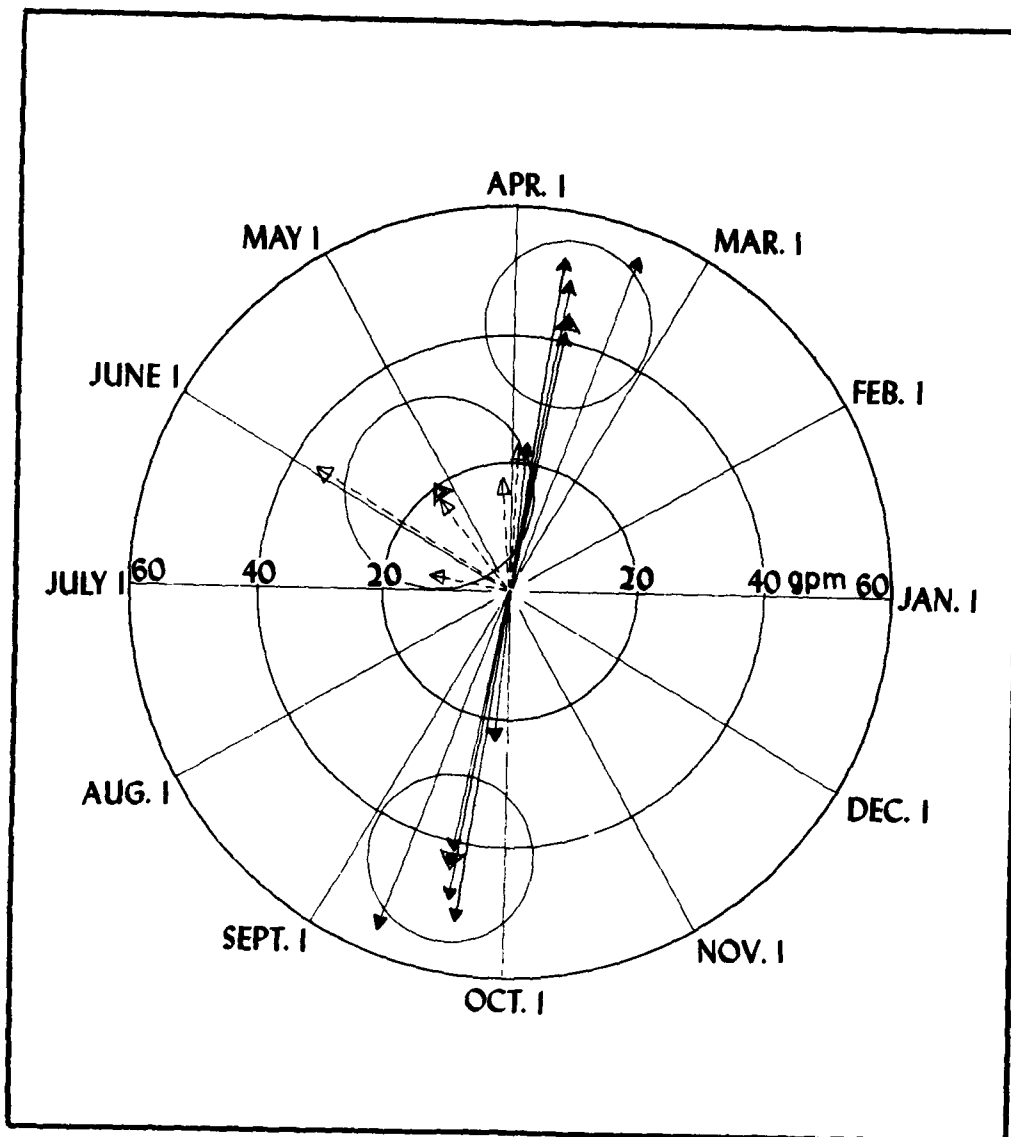


Figure 3. Harmonic dial for the yearly march of the 300-700 mb thickness difference ($50 - 80^{\circ}$ S). Amplitudes and dates of the occurrence for the maxima for each of the five 12-month series (April 1957 through March 1962) and the mean series are represented by: open triangles—first harmonic; solid triangles—second harmonic; double triangles—5-year mean series. The circles around the end point of the mean series are drawn with a radius equal to the standard vector deviation computed for the five 12-month series.

3. Heat flux from the surface: This term of the atmospheric heat budget will also be considered only with regard to its meridional differences, in order to determine if its yearly variation possesses a second or higher harmonic component which is larger than its first. This question can be answered by referring to Table 5, which gives the monthly values of the surface temperature difference (middle minus polar latitudes). To compute these mean meridional differences, the averages for eight stations located between 47 and 54° S and at widely different longitudes, which have been tabulated by Fabricius (1957), were used for the middle latitudes, and the seven-year averages of Belgrano Base (78° S, Weddel Sea area) and Little America (78° S, Ross Sea) for the polar regions.

Table 5. Mean monthly differences of the surface temperature (51 minus 78° S in °C)

<u>I</u>	<u>II</u>	<u>III</u>	<u>IV</u>	<u>V</u>	<u>VI</u>	<u>VII</u>	<u>VIII</u>	<u>IX</u>	<u>X</u>	<u>XI</u>	<u>XII</u>
14	20	29	33	34	33	37	37	37	27	20	13

Mean: 28° C. Harmonic components:

$r_1 = 11.2^\circ \text{C}$; $\phi_1 = 266^\circ$; maximum at July 4.

$r_2 = 4.4^\circ \text{C}$; $\phi_2 = 289^\circ$; maxima at March & Sept. 22.

variance higher harmonics/total variance: $R = 0.01$.

Although the heat flux from the surface to the atmosphere is not an important factor of the heat budget of the troposphere at polar latitudes, it can be so at middle latitudes over the southern oceans. It should be

noted that the relatively large amplitude of r_2 in the yearly march of the meridional temperature differences is mainly due to the existence of a large value of r_2 in the polar regions. For the yearly march of the temperature at the middle latitude stations, the second harmonic component is quite unimportant.

Table 6. Harmonic components of the yearly march of mean surface temperatures

		51° S (max. at)	78° S (max. at)
Yearly Mean:	$t_m =$	4.7° C	-23.2° C
First Harmonic:	$r_1 =$ $\phi_1 =$	2.6° C 59° (Feb. 1)	14.0° C 81° (Jan. 9)
Second Harmonic	$r_2 =$ $\phi_2 =$	0.3° C (March + 332° Sept. 1)	4.4° C (March + 292° Sept. 20)
Variance higher harmonics			
Total variance		.001	.003

C. Seasonal variations of the meridional temperature gradients and the strength of the circumpolar vortex

From the above results, it can be stated that only above the surface in the troposphere is the semi-annual component dominant in the yearly march of the meridional temperature gradients between middle and polar latitudes. This result is summarized in Table 7. The first line of this table refers to the data discussed in the preceding section; the second and third to the thickness differences computed from the latitudinal

Table 7. Ratio of the amplitudes of the second and first harmonic of the yearly march of the meridional temperature differences

<u>Latitudes</u>	<u>Level or Layer</u>	<u>r_2/r_1</u>
51-78° S	surface	0.3
50-80	300-700 mb	<u>2.3</u>
50-80	100-300 mb	0.16
51-80	100-200 mb	0.14
51-80	100 mb	0.15

means described in the legend to Fig. 2 and with more detail in (Schwerdtfeger, 1962); the fourth and fifth to the 100-200 mb thickness and the 100 mb temperature differences between Port Stanley and Byrd, two representative stations for which reliable 5-year series were readily available (Climat temp transmissions from Port Stanley and Monthly Climatic Data for the World). It is obvious that in the stratosphere the second harmonic loses importance in comparison to the first. However, it is the superposition of the tropospheric and the stratospheric thickness pattern which determines the behavior of the circumpolar vortex in the stratosphere. Therefore, the semi-annual periodicity of the differential heating of the troposphere is important for the behavior of the entire circumpolar vortex. It can be considered as one of the forcing factors which tend to re-establish the pole-centered vortex of the southern hemisphere after cyclonic developments in the strong circumpolar westerlies have temporarily disturbed its nearly circular symmetric features. It causes a strengthening of the circumpolar

vortex until September. Only after then, that is from October on, do both components of the differential heating (annual and semi-annual) tend to decrease the strength of the vortex. At this time the vortex breaks down in the stratosphere and weakens in the troposphere.

An inspection of the aerological observations for the years 1957 to 1961 indicates that the real southern circumpolar vortex behaves in this manner. This phenomenon is substantiated by Fig. 4 and also by Table 8, which refers to the monthly mean height differences between the three middle latitude stations located near 50° S and the South Pole station, at several isobaric levels up to 100 mb. For the 50 mb level, the available observations were not sufficient to compute a reliable series of monthly height differences. Tentatively, only the values for January and September were determined by extrapolation; these are marked in Fig. 4 by small circles. Since all these data have been computed from the series of monthly means, no great exactness is claimed, in particular not for the date of occurrence of the maxima. However, the general trend towards the September maximum is beyond doubt. More evidence for this phenomenon and its relation to the very conspicuous seasonal variations of atmospheric pressure at surface has been published by Schwerdtfeger (1962). In the present paper, the principal aim has been to show that the predominance of the semi-annual periodicity in the yearly march of the meridional temperature gradient of the troposphere is a characteristic which distinguishes the southern from the northern polar vortex. This is caused by the effect of the geographical

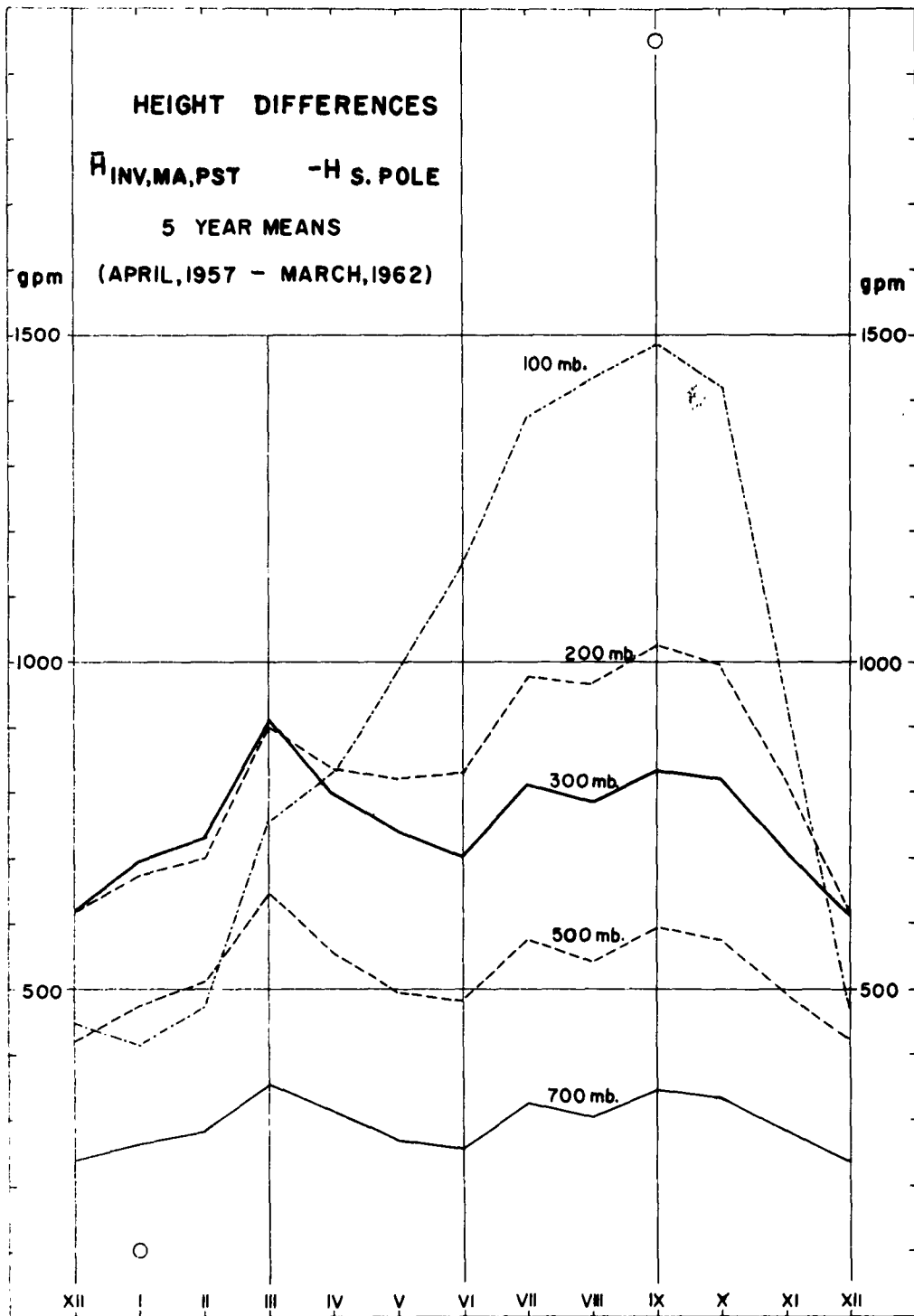


Figure 4. Annual march of the mean height differences, (Port Stanley + Marion + Invercargill)/3 minus South Pole, for the 5 years, April 1957 through March 1962. Estimated values for the 50 mb level are indicated by small circles for January and September.

Table 8. Characteristics of the yearly march of the height differences at isobaric levels between 50°S and the South Pole (5-year averages)

Level	Mean (gpm)	Annual component max. at r_1 (gpm)		Semi-annual component max. at r_2 (gpm)		Ratio r_2/r_1	Date of max. of annual + semi-annual component
700	298	14	Aug. 3	41	March + Sept. 16	2.9	Sept. 13
500	529	27	June 28	67	March + Sept. 16	2.5	Sept. 11
300	763	38	June 22	86	March + Sept. 17	2.2	Sept. 10
200	847	138	Aug. 4	99	March + Sept. 21	0.7	Sept. 10
100	975	512	Aug. 10	162	March + Sept. 27	0.3	Sept. 6

features of the two hemispheres on the heat budget of the atmosphere. It should be noted that in the northern hemisphere a semi-annual periodicity, though much weaker, can be found in the meridional thickness differences, as was mentioned by Scherhag (1948). In the northern hemisphere, however, the differential heating effect cannot show as much circular symmetry as it does in the southern regions. At least three processes (absorption of solar radiation, infrared cooling, and net latent heating) are decisively different over continents and oceans, and the tendency to re-establish a circumpolar vortex following some kind of

disorder must be much less effective in the northern than in the southern hemisphere.

Referring to the observed facts that the northern circumpolar vortex can break down at any time between the winter solstice and spring equinox (Warnecke 1962, Fig. 17), while this did not happen to the southern vortex in the eight years with adequate aerological observations, and also having in mind the studies of C. E. Palmer (1959) and Boville et al. (1961) concerning this subject, there remains the following question: Can it be shown through dynamic theory of large scale atmospheric motion and with realistic assumptions as to the characteristics of the two polar vortices, that a strongly asymmetric vortex proves unstable and a symmetric one stable in its reaction to a (not necessarily small) disturbance?

D. Conclusions

1. An examination of the various terms of the heat budget of a quasi-planetary atmosphere indicates that the absorption of solar radiation is the only term which can produce, in the troposphere, a pronounced semi-annual variation of the mean meridional thickness gradient between middle and polar latitudes.
2. The atmosphere of the extratropical regions of the southern hemisphere may be considered as quasi-planetary.
3. The semi-annual periodicity of the mean tropospheric meridional thickness gradient also contributes to the seasonal change of the strength of the circumpolar vortex in the stratosphere.

4. Superposition of the annual and the semi-annual component of the yearly march of the circumpolar westerlies explains why the maximum intensity of the vortex is found in September (spring equinox).

5. Only after the September peak does the combined effect of terms which make up the differential heating of the atmosphere vary in such a way that the vortex weakens significantly. Only then can the spring warming of the polar stratosphere "break" the vortex.

6. In the northern hemisphere a semi-annual variation of the meridional thickness gradient also exists. There, however, the various terms of the atmospheric heat budget show far less pole-centered symmetry, and so does the polar vortex itself. The differential heating processes which tend to re-establish circular symmetry after a disturbance can be weaker than the asymmetrically operating ones. Therefore, the northern vortex may prove less stable than its southern counterpart.

REFERENCES

- Alt, Astapenko and Ropar, Some aspects of the Antarctic atmospheric circulation in 1958, IGY Report No. 4, National Academy of Sciences, World Data Center A, Washington, D. C., 1959.
- Boville, Wilson and Hare, Baroclinic waves of the polar night vortex, Journal of Meteorology, 18, No. 5, October 1961.
- Davis, P. A., A re-examination of the heat budget of the troposphere and lower stratosphere, Scientific Report No. 3, College of Engineering, New York University, October 1961.
- Fabricius, A. F., Climate of the sub-Antarctic islands, Chapter 7 in Meteorology of the Antarctic, edited by M. P. van Rooy, Weather Bureau Pretoria, South Africa, 1957, p. 123.
- Farkas, E., Springtime temperature changes in the Antarctic stratosphere, New Zealand Journal of Geology and Geophysics, 4, No. 4, 1961.
- Gabites, J. F., The heat balance of the Antarctic through the year, Proceedings of the Symposium on Antarctic Meteorology, Melbourne, 1959.
- Korb, Michalowski and Möller, Investigations on the heat balance of the troposphere, Technical Report No. 1, Meteorolog.-Geophys. Institut, Universität Mainz, August 1956.
- MacDowall, J., Some observations at Halley Bay in seismology, glaciology and meteorology, Proceedings of the Royal Society, A 256, 1960, pp. 149-197.

- Möller, F. , Der Strahlungshaushalt der Troposphäre, Meteorologische Rundschau, 13, Heidelberg 1960, p. 65.
- Moreland, W.B. , Antarctic stratospheric circulation and ozone observations, Proceedings of the Symposium on Antarctic Meteorology, Melbourne, 1959.
- Myers, V.A. , Precipitable water, Bulletin of the American Meteorological Society, 43, June 1962.
- Ohring, G. , The radiation budget of the stratosphere, Journal of Meteorology, 15, No. 5, October 1958.
- Palmer, C.E. , The stratospheric polar vortex in winter, Journal of Geophysical Research, 64, No. 7, July 1959.
- Palmer, C.E. , and R. C. Taylor, The vernal breakdown of the stratospheric cyclone over the South Pole, Journal of Geophysical Research, 65, No. 10, October 1960.
- Rastorguev, V.I. , and J.A. Alvarez, Description of the Antarctic circulation from April to November 1957, IGY Report No. 1, National Academy of Sciences, World Data Center A, Washington, D. C. , 1958.
- Scherhag, R. , Neue Methoden der Wetteranalyse und Wetterprognose, Springer Verlag, Berlin, Göttingen, Heidelberg, 1948.
- Schwerdtfeger, W. , The seasonal variation of the strength of the southern circumpolar vortex, Monthly Weather Review, 88, No. 6, June 1960.

Schwerdtfeger, W., Die halbjährige Periode des meridionalen Temperaturgradienten in der Troposphäre und des Luftdrucks am Boden im Südpolargebiet, ihre Erscheinungsform und kausalen Zusammenhänge, in press, Beiträge zur Physik der Atmosphäre, Weickmann-Band, 1962.

Van Loon, H., Charts of average 500 mb absolute topography and sea level pressures in the Southern Hemisphere in January, April, July and October, NOTOS, 10, Pretoria, South Africa, 1961, pp. 105-112.

Warnecke, G., Ueber die Zustandsänderungen der nordhemisphärischen Stratosphäre, Meteorologische Abhandlungen des Instituts für Meteorologie und Geophysik der Freien Universität Berlin, 28, No. 3, 1962.

THE RELATION BETWEEN ATMOSPHERIC ENTROPY
AND AVAILABLE POTENTIAL ENERGY

John A. Dutton

Abstract. The concept of available potential energy as defined by Lorenz [1955] separates the total potential energy (internal plus gravitational potential energies) into a portion available for conversion to kinetic energy and a portion not available.

It is shown that available potential energy represents the amount of gravitational potential energy which must be expended to bring the isobars and isentropes to their average height and thus produce a pressure and potential temperature distribution with only vertical variation. An expression is derived from this definition which agrees with those of previous authors.

The reference state of the atmosphere specified by this definition possesses the maximum entropy on every horizontal surface which can be obtained by isentropic processes which do not change the average height distribution of potential temperature. The amount of available

potential energy is therefore expressed as a weighted average of the difference in local entropies between an actual and the reference state of the atmosphere.

It is shown that approximations which are valid on the global scale allow the time rate of change of available potential energy to be expressed as a weighted average of the local rate of change of the entropy.

This formulation shows that the concept of entropy provides a basis in classical and statistical physics for the meteorological concept of available potential energy.

1. Introduction

The study of atmospheric motions is in part concerned with the transformations between the three forms of energy presently considered important to the general circulation — kinetic, internal, and gravitational potential energy. The sum of the last two is known as the total potential energy, the sum of the three as the total energy of the atmosphere. The amount of these forms of energy in the atmosphere is shown by Table 1, adapted from computations by Spar [1949].

The emphasis in studies of energy transmutations has been on the question of how total potential energy is transformed into kinetic energy to replace the kinetic energy dissipated by friction. A major advance in the clarification of this problem was made by Lorenz [1955] (hereafter referred to without date) in expanding Margules' [1904] original separation of the total potential energy into a portion available for conversion into kinetic energy and a portion not available for conversion. Lorenz' work was extended by Van Mieghem [1956, 1957] (hereafter referred to without date).

Lorenz pointed out that the addition or removal of heat differentially may produce pressure gradients which will accelerate the wind and increase the kinetic energy. He defined the available potential energy as the difference between the total potential energy of an arbitrary

atmosphere and that which would exist after adiabatic redistribution of the mass so that a stable horizontal stratification was realized. Using assumptions not contained in this definition (see Van Mieghem), Lorenz derived a series of analytical expressions for the amount of available potential energy.

Van Mieghem attempted to work directly from definition, and took both hydrostatic and hydrodynamic equilibrium as reference states from which to compute the available potential energy. For the case of hydrostatic equilibrium, he found an additional small term not contained in Lorenz' expressions.

In an earlier effort to explain the maintenance of the general circulation of the atmosphere, Lettau [1954] (hereafter referred to without date) considered an average heat budget for the main layer of weather activity. He found that the net heating of the atmosphere is zero, but that the geometry of the earth-sun relationship produces heating in the warm regions and cooling in the cool regions of the earth, and therefore, a rate of entropy decrease of 2 watts/m^2 . He postulated that the total entropy of the atmosphere is constant, and that the work of the wind against friction provides the necessary increase in entropy. White and Saltzman [1956], using observational data to calculate values of the rate of conversion between total potential and kinetic energy, estimated a frictional dissipation of 5 watts/m^2 .

Table 1. The reservoirs of atmospheric energy (20° N to 70° N) as computed by Spar [1949].

	<u>January</u>	<u>July</u>	<u>January-July</u>
Internal	550.0 $\frac{\text{k watt-hr}}{\text{m}^2}$	568.0 $\frac{\text{k watt-hr}}{\text{m}^2}$	-18.0 $\frac{\text{k watt-hr}}{\text{m}^2}$
Potential	218.0	227.0	-9.0
Kinetic	0.515	0.110	+0.405

Values obtained from Spar's data by conversion to kilowatt-hours and dividing by the area of the globe between 20° N and 70° N.

Purpose. It is the purpose of this paper to show that these two approaches, as exemplified by the work of Lorenz and Lettau, have much in common. To do so, it will be necessary to re-examine the definition and concept of available potential energy as previously developed by Lorenz and Van Mieghem. We shall show that:

(1) Available potential energy can be defined as the difference of the gravitational potential energies of an actual or arbitrary state of the atmosphere and a reference state determined by averages and reached by isentropic processes.

(2) The entropy on each horizontal surface of the reference state is the maximum which can be obtained by isentropic processes which do not affect the average height distribution of potential temperature.

(3) The amount of available potential energy found with (1) is equal to the average of the local difference of the entropies in the two states multiplied by a function of the stability of the reference state.

(4) On the global scale, the time rate of change of available potential energy is a weighted average of the local rate change of the entropy.

The derivation based on (1) will produce an analytical expression for the amount of available potential energy which is identical with Van Mieghem's result, whose derivation is more complex.

2. Fundamental Concepts and Equations

Integrals of the form (see Table of Symbols)

$$\int f(\lambda, \phi, z, t) \rho \delta \tau$$

may be differentiated with respect to time by the relation

$$\frac{d}{dt} \int f \rho \delta \tau = \int \frac{df}{dt} \rho \delta \tau \quad .$$

This is justified by noting that $\rho \delta \tau$ is invariant under atmospheric motion by the equation of continuity, for

$$\frac{d}{dt} (\rho \delta \tau) = \delta \tau \left(\frac{d\rho}{dt} + \rho \nabla \cdot \underline{V} \right) \equiv 0$$

because of the definition of divergence

$$\delta \tau \nabla \cdot \underline{V} = d(\delta \tau)/dt \quad .$$

This result is equivalent, using the equation of continuity, to the theorem that the total derivative of a parametric integral is computed by partial

differentiation of the integrand, provided: (1) that the limits of integration are not functions of the parameter; (2) that the net advection through the boundaries is zero; and (3) that appropriate continuity requirements are satisfied by the integrand and its partial derivatives.

Energy Equation. The first law of thermodynamics for dry, viscous fluids

$$\rho \frac{dq}{dt} = C_v \rho \frac{dT}{dt} + p \frac{\partial v_j}{\partial x_j} - \frac{\partial v_i}{\partial x_k} \Delta_{ik}(\mu) \quad (1)$$

(where the Stokes dissipation term is expressed in conventional tensor notation) combines with the Navier-Stokes equation and the equation of continuity to produce the atmospheric energy equation

$$\frac{dK}{dt} + \frac{d\Pi}{dt} = \frac{d}{dt} \int \rho q \delta\tau + \int \frac{\partial}{\partial x_k} [v_i \Delta_{ik}(\mu)] \delta\tau \quad (2)$$

for the rate of change of the kinetic energy K and the total potential energy Π . Since $\frac{\partial}{\partial x_k} [v_i \Delta_{ik}] = \nabla \cdot (Y \cdot \underline{\Delta}(\mu))$, where $\underline{\Delta}$ is a second order tensor, Gauss' theorem allows the last term of (2) to be written as

$$\oint [Y \cdot \underline{\Delta}(\mu)] \cdot N \delta\sigma$$

which for the atmosphere may be reduced to

$$\oint \mu \left[v_i \frac{\partial v_i}{\partial z} + v_i \frac{\partial v_3}{\partial x_i} - \frac{2}{3} v_3 \frac{\partial v_j}{\partial x_j} \right] d\sigma_e$$

where σ_e is the earth's surface and v_3 the vertical component of the wind. The dominant term in most cases is the first, so that

$$\frac{dK}{dt} + \frac{d\Pi}{dt} = \frac{d}{dt} \int \rho q \delta \tau - \oint \mathbf{V} \cdot \boldsymbol{\tau} d\sigma_e \quad (3)$$

The last term represents the frictional effects at the earth's surface. For mechanically and thermally insulated systems, the right side of (3) vanishes and the total energy ($K + \Pi$) is constant. The notion that kinetic energy increases result from decreases of total potential energy is thus valid to the extent that the two terms on the right of (3) cancel for large scale atmospheric processes.

Entropy Equations. For viscous fluids, the rate of change of entropy may be defined as

$$T \frac{dS}{dt} = \frac{dq}{dt} + \alpha \frac{\partial v_i}{\partial x_k} \Delta_{ik}(\mu) \quad (4)$$

so that use of (1) and the equation of continuity and the equation of state gives

$$\frac{dS}{dt} = \frac{C_p}{T} \frac{dT}{dt} - \frac{R}{p} \frac{dp}{dt} = C_p \frac{d}{dt} \ln \theta$$

and finally, the meteorological form

$$S = C_p \ln \theta + \text{const} \quad (5)$$

We shall take the same reference for all determinations of entropy so that the constant in (5) is always the same. The definition of entropy in (5) may be considered as valid for parcels small enough that they are homogeneous. The entropy S^* on a horizontal surface is the sum of parcel entropies and thus given by

$$S^* = \int S \delta A = C_p \int \ln \theta \delta A + \text{area} \cdot \text{const}$$

and since

$$\ln [1 + x] \leq x \quad (-1 \leq x)$$

we find for $\theta = \bar{\theta} + \theta'$,

$$S^*(\theta) - S^*(\bar{\theta}) = C_p \int \ln \left[1 + \frac{\theta'}{\bar{\theta}} \right] \delta A \leq C_p \int \frac{\theta'}{\bar{\theta}} \delta A = 0 \quad (6)$$

and thus the entropy on a surface is a local maximum when $\theta = \bar{\theta}$ everywhere on the horizontal surface. In particular this is the maximum which can be obtained by isentropic processes which do not change the average vertical distribution of potential temperature. By the same sort of argument the adiabatic atmosphere with $\bar{\theta}(z)$ constant possesses the maximum entropy which can be obtained without the addition of heat to the atmosphere.

It is important to note that the entropy of the atmosphere may change even though the entropy of each parcel of air which moves isentropically is conserved.

3. Available Potential Energy

In this section, the proposed definition for available potential energy will be stated and examined. It specifies the physical processes necessary to reach the reference state more explicitly than previous definitions, and reveals some interesting properties of available potential energy.

Let us define the amount of the available potential energy in an actual state of the atmosphere as the difference in the gravitational potential energies of that state and a reference state, reached by an

isentropic process, in which $\theta = \bar{\theta}$ and $p = \bar{p}$ on every horizontal surface.

Among the consequences of this definition are the following:

(1) The internal energy I

$$I = \int \frac{C_v}{R} p \delta \tau = \text{Area} \int \frac{C_v}{R} \bar{p}(z) dz$$

is the same in both the arbitrary and reference states.

(2) The available potential energy is a function of the difference in the density or mass distributions of the two states. Every parcel with potential temperature θ must move to a level where that θ is the average, and the pressure upon arrival at that level must be the average pressure at that level. Thus the density in the reference state is determined by a Poisson relation, and available potential energy is a measure of the gravitational potential energy expended in accomplishing the required changes.

(3) The reference state is completely determined by the vertical distribution of the horizontal averages of pressure and potential temperature in the arbitrary state. Hence the available potential energies in two actual states can be compared since the potential energy of their reference states can be compared. (Note the difference between this definition of reference state and Lorenz' "horizontal, stable stratification," and Van Mieghem's "hydrostatic equilibrium" in which many reference states are possible.)

(4) If the atmosphere is homogeneous (constant density) there is no available potential energy.

(5) Available potential energy cannot be defined if the reference state is adiabatic and the arbitrary state has no local instabilities.

(6) In view of eq (6), available potential energy is simply the amount of gravitational potential energy expended in bringing all the isobars to their average position and maximizing the entropy of every surface. Therefore, if the arbitrary state has no local instabilities ($\partial\theta/\partial z \geq 0$ everywhere) and since isentropes may be considered continuous, the requirement that $\bar{\theta}(z)$ is constant for an adiabatic reference atmosphere implies that θ be the same everywhere in the arbitrary state. Hence, the reason for the failure of the concept in (5) above is that the entropy is already the maximum which can be obtained without changes in the internal energy.

(7) Except for the nugatory case of density increasing with height in the reference atmosphere, the available potential energy is always non-negative if it is defined. This is obvious since it represents work done to maximize the entropy.

Derivation. Two assumptions (in addition to a dry atmosphere) are necessary to produce a simple derivation of an analytical expression for the amount of available potential energy in the atmosphere. The first is that variations in radial distance from the earth's center are negligible in computing the surface area of a given horizontal or geopotential level.

This introduces less than a 2.0 per cent error in view of the fact that the ratio $(a + z)^2/a^2$ is less than 1.02 even if we go as high as $z = 60$ km. Hence

$$\delta\tau = a^2 \cos \phi \, d\phi \, d\lambda \, dz = a^2 \delta A \, dz \quad .$$

The second assumption is that the atmosphere is close enough to its average state that a linear approximation may be used. (Van Mieghem used the same linearization as a last step in his derivation.)

In the arbitrary state there are parcels at level z_a a distance Δz away from their position z_r in the reference state. We take $\Delta z = z_r - z_a > 0$ if upward motion to the reference position is required. Then, in view of the linear hypothesis, the values of the thermodynamic variables in each parcel at a point in the arbitrary state may be expressed in terms of the values in the reference state at the same point. That is,

$$\theta' = \theta - \bar{\theta} = \frac{\partial \bar{\theta}}{\partial z} \Delta z \quad (7a)$$

$$p' = p - \bar{p} = \frac{\partial \bar{p}}{\partial z} \Delta z \quad (7b)$$

$$\rho - \rho_r = \frac{\partial \rho_r}{\partial z} \Delta z \quad (7c)$$

where, by Poisson's relations,

$$\rho_r = \text{const} \frac{\bar{p}}{\bar{\theta}^{C_v/C_p}} \quad (8)$$

so that

$$\frac{\partial \rho_r}{\partial z} = \rho_r \left\{ \frac{C_v}{C_p} \frac{1}{p} \frac{\partial \bar{p}}{\partial z} - \frac{1}{\bar{\theta}} \frac{\partial \bar{\theta}}{\partial z} \right\} \quad (9)$$

Physically, we propose to find a parcel in the arbitrary state with $\theta = \bar{\theta}$ and move it to z_r , changing its pressure to \bar{p} without changes in its potential temperature. The density must then change in accord with the Poisson equation (8).

Thus the amount of available potential energy may be expressed as

$$A = \int g [\rho(z) - \rho_r(z)] z \delta \tau \quad (10)$$

and it is clear that its existence depends on the condition that

$$\rho(z) \neq \rho_r(z) .$$

We shall return to the direct evaluation of (10) later. First, however, we shall choose to measure the change in height of the same density surface in the two states since an integration by parts gives

$$\int g \rho z dz = \left[g \frac{z^2}{2} \rho(z) \right]_0^Z - \int_0^Z g \frac{z^2}{2} d\rho(z) \quad (11)$$

in which the constant term vanishes at the bottom ($z = 0$) and the "top" ($\rho(Z) = 0$) of the atmosphere. Thus

$$\begin{aligned} A &= \int a^2 \left[\int g \left[\frac{z_r^2(\rho_r) - z_a^2(\rho_r)}{2} \right] d\rho_r \right] \delta A \\ &= \int a^2 \left[\int g \left[\frac{z_r^2 - (z_r - \Delta z)^2}{2} \right] \frac{\partial \rho_r}{\partial z_r} dz_r \right] \delta A \\ &= - \int g \left[\frac{(\Delta z)^2}{2} - \Delta z z_r \right] \left(\frac{\partial \rho_r}{\partial z_r} \right) \delta \tau \end{aligned}$$

The second term of the last equation vanishes on every horizontal surface, so that using (7a) to determine Δz , we find

$$A \cong -\int g \frac{(\theta')^2}{2} \left[\frac{\partial \rho_r}{\partial z} / \left(\frac{\partial \bar{\theta}}{\partial z} \right)^2 \right] \delta \tau \quad (12)$$

The quantity in square brackets is a function of the stability of the equilibrium states. Substitution of (8) and noticing that with (7a) and (7b),

$$(\rho')^2 / \bar{p} \frac{\partial \bar{p}}{\partial z} = \left(\frac{1}{\bar{p}} \frac{\partial \bar{p}}{\partial z} \right) (\theta')^2 / \left(\frac{\partial \bar{\theta}}{\partial z} \right)^2 \quad (13)$$

we obtain the expression

$$\begin{aligned} A &\cong \int \frac{1}{2} \frac{(\theta')^2}{\left(\frac{\partial \bar{\theta}}{\partial z} \right)^2} \left[\frac{1}{\bar{\theta}} \frac{\partial \bar{\theta}}{\partial z} - \frac{C_v}{C_p} \frac{1}{\bar{p}} \frac{\partial \bar{p}}{\partial z} \right] g \rho_r \delta \tau \\ &\cong \int \left[\frac{(\theta')^2}{\frac{\partial \bar{\theta}^2}{\partial z}} + \frac{C_v}{C_p} \frac{(\rho')^2}{\left(-\frac{\partial \bar{p}^2}{\partial z} \right)} \right] g \rho_r \delta \tau \end{aligned} \quad (14)$$

This is identical with Van Mieghem's result [Eq. 5.7a, 1956] except for the difference in reference states; the first term (potential temperature) is equivalent to one of Lorenz' expressions [Eq. 8, 1955] which were derived in (x, y, p) coordinates.

Van Mieghem has shown that the second term (pressure) is about 10 per cent of the magnitude of the potential temperature term, and this estimate of size can be verified by direct calculation of numerical examples.

If the atmosphere is homogeneous then $\rho_r = \text{const } \rho$, and $\partial \rho_r / \partial z = 0$, so that (12) implies that $A = 0$, thus justifying statement (4).

If the reference state is adiabatic ($\partial\bar{\theta}/\partial z = 0$) and the arbitrary state is not, then there exist parcels with $\theta \neq \bar{\theta}$ which have no place in the reference state. If the arbitrary state is also adiabatic, then (12) has a division of zero by zero, and A is undefined, as mentioned in statement (5).

A Modified Form. If the reference state is in hydrostatic equilibrium

$$\frac{\partial \bar{p}}{\partial z} = -g\rho_r$$

then (9) may be written

$$-\frac{\partial \rho_r}{\partial z} = \frac{\rho_r}{T_r} \left\{ \frac{T_r}{\bar{\theta}} \frac{\partial \bar{\theta}}{\partial z} + \frac{C_v g}{C_p R} \right\} \quad (15)$$

and since under hydrostatic equilibrium

$$\frac{T_r}{\bar{\theta}} \frac{\partial \bar{\theta}}{\partial z} = \gamma_d - \gamma_r \quad (16)$$

(15) becomes

$$\begin{aligned} -\frac{\partial \rho_r}{\partial z} &= \frac{\rho_r}{T_r} \left\{ \gamma_d - \gamma_r + \frac{C_v}{R} \gamma_d \right\} \\ &= \frac{\rho_r}{T_r} \left\{ \frac{C_p}{R} \gamma_d - \gamma_r \right\} = \frac{\rho_r}{T_r} [\gamma_h - \gamma_r] \end{aligned} \quad (17)$$

where γ_r is the lapse rate of the reference state, γ_d is the dry adiabatic lapse rate, and γ_h is the autoconvective lapse rate of a homogeneous atmosphere.

Now (14) may be rewritten, using (16) and (17), to read

$$A \cong \int \frac{(\theta')^2}{2} \frac{[\gamma_h - \gamma_r]}{(\gamma_d - \gamma_r)^2} T_r g \rho_r \delta \tau \quad (18)$$

Since

$$T_r = \frac{\bar{R}/C_p}{\bar{\theta}(p)} \frac{R/C_p}{p/(p_0)}$$

$$\rho_r = \frac{(\bar{p}) \frac{C_v/C_p}{p} \frac{R/C_p}{(p_0)}}{R \bar{\theta}}$$

and thus

$$\bar{p} = R \rho_r T_r$$

we may express (18) in a form to facilitate computation as

$$A \cong \int \frac{(\theta')^2}{2} \frac{[\gamma_h - \gamma_r]}{(\gamma_d - \gamma_r)^2} \gamma_h \bar{p} \delta \tau \quad (19)$$

4. Available Potential Energy as an Entropy Difference

Since the definition of available potential energy implies that the entropy is the same or larger on every horizontal surface in the reference state, it seems reasonable to expect that the amount of available energy can be expressed as an entropy difference.

At each point in the two states, the parcel entropy is given by (5), so that for the difference in entropy at a point in the two states we find

$$\Delta_r S = C_p [\ln \theta(x, y, z) - \ln \bar{\theta}(z)]$$

$$= C_p \ln [1 + (\theta'/\bar{\theta})]$$

Because we may safely take $|\theta'/\bar{\theta}| < 1$, the expansion of (19) in an infinite series yields

$$\Delta_r S = C_p \left\{ \frac{\theta'}{\bar{\theta}} - \frac{1}{2} \left(\frac{\theta'}{\bar{\theta}} \right)^2 + \frac{1}{3} \left(\frac{\theta'}{\bar{\theta}} \right)^3 - \dots \right\} \quad (20)$$

Typical values of θ' at 500 mb are $\pm 15^\circ \text{C}$ compared with $\bar{\theta} = 300^\circ \text{K}$, so we estimate that

$$\frac{1}{2} \left(\frac{\theta'}{\bar{\theta}} \right)^2 \cong 1.2 \cdot 10^{-3} ; \quad \frac{1}{3} \left(\frac{\theta'}{\bar{\theta}} \right)^3 \cong 4.0 \cdot 10^{-5}$$

and hence (20) is represented by its first two terms to a greater accuracy than one order of magnitude. Because the integral of $(\theta'/\bar{\theta})$ will vanish on every horizontal surface, we may write (12), in view of the two-term approximation to (20), as

$$A \cong \int \frac{\Delta_r S}{C_p} \left[\frac{1}{\rho_r} \frac{\partial \rho_r}{\partial z} / \left(\frac{\partial \bar{\theta}}{\partial z} \right)^2 \right] g \rho_r \delta \tau \quad (21)$$

or with the hydrostatic approximation

$$A = \int -\Delta_r S \frac{[\gamma_h - \gamma_r]}{(\gamma_d - \gamma_r)^2} \gamma_d \frac{\bar{p}}{R} \delta \tau \quad (22)$$

It is possible to use entropy to give another and revealing formulation to the amount of available potential energy. Let us consider a new reference state (denoted by the subscript s) defined in terms of \bar{p} and $\bar{\rho}$ so that each parcel has a reference potential temperature of

$$\theta_s = \frac{\text{const } \bar{p}^{-C_v/C_p}}{\bar{\rho}} \quad (23)$$

In this case, the total potential energy is the same in both the arbitrary and the reference state, but the flow to the reference state does not necessarily preserve parcel entropy. We note that because of (8) and (23),

$$\rho_r \bar{\theta} = \theta_s \bar{\rho} \quad (24)$$

Thus the difference in entropy between the two states at a point may be written

$$\begin{aligned}\Delta_s S &= C_p [\ln \theta - \ln \theta_s] \\ &= C_p [\ln \theta - \ln \bar{\theta}] + C_p \ln(\bar{\theta}/\theta_s) \\ &= \Delta_r S + C_p \ln(\bar{\rho}/\rho_r)\end{aligned}\quad (25)$$

Now (21) may be expressed as

$$A = \int [\Delta_s S - \ln(\bar{\rho}/\rho_r)] \left[\frac{g}{C_p} \frac{\partial \bar{\rho}}{\partial z} / \left(\frac{\partial \bar{\theta}}{\partial z} \right)^2 \right] \delta \tau \quad (26)$$

If A is positive, we see from (10) that $\bar{\rho} > \rho_r$ at least on some surfaces, so that $\ln(\bar{\rho}/\rho_r) > 0$ at some levels. With this result, it is clear from (25) or (26) that the change in entropy $\Delta_s S$ is not as large as the change $\Delta_r S$ on some surfaces. Thus we may conclude that the entropy cannot be maximized on every surface until some of the potential energy is utilized in the process.

To attempt to show directly that $\bar{\rho} \geq \rho_r$, we shall return to (10) and calculate the amount of available potential energy in terms of variances and covariances. This will yield an expression which may be calculated to any desired accuracy and which does not depend on the linearization used in the previous section. Taking the integral on every horizontal surface

$$A_z = \int g(\rho - \rho_r) \delta A \quad (27)$$

so that from (10)

$$A = \int A_z z dz \quad (28)$$

Since in this formulation

$$A_z = \text{Area } g [\bar{\rho} - \rho_r] \quad , \quad (29)$$

we shall calculate the difference of the two densities on every surface.

By definition

$$\begin{aligned} \bar{\rho} - \rho_r &= \text{const} \left[\overline{\left(\frac{C_v/C_p}{\theta} \right)} - \frac{\overline{C_v/C_p}}{\bar{\theta}} \right] \\ &= \rho_r \left\{ \left[\frac{(1 + p'/\bar{p})^{1-\kappa}}{(1 + \theta'/\bar{\theta})} \right] - 1 \right\} \quad (\kappa = R/C_p) \end{aligned} \quad (30)$$

Because we may assume $|\theta'/\bar{\theta}| < 1$ and $|p'/\bar{p}| < 1$, (30) may be expanded in an infinite series and yields

$$\bar{\rho} - \rho_r = \rho_r \left[\left(1 - \frac{\theta'}{\bar{\theta}} + \left(\frac{\theta'}{\bar{\theta}} \right)^2 - \dots \right) \left(1 + (1-\kappa) \frac{p'}{\bar{p}} - \frac{(1-\kappa)\kappa}{2} \left(\frac{p'}{\bar{p}} \right)^2 + \dots \right) - 1 \right]$$

which after integrating out the single deviations and ignoring third order products (triple correlations) gives

$$\bar{\rho} - \rho_r = \rho_r \left[\overline{\left(\frac{\theta'}{\bar{\theta}} \right)^2} - \frac{(1-\kappa)\kappa}{2} \overline{\left(\frac{p'}{\bar{p}} \right)^2} - (1-\kappa) \overline{\left(\frac{\theta'}{\bar{\theta}} \frac{p'}{\bar{p}} \right)} \right] \quad (31)$$

so that for $R/C_p = 2/7$ and $C_v/C_p = 5/7$

$$A_z \cong \int \left[\left(\frac{\theta'}{\bar{\theta}} \right)^2 - \frac{5}{49} \left(\frac{p'}{\bar{p}} \right)^2 - \frac{5}{7} \overline{\left(\frac{\theta' p'}{\bar{\theta} \bar{p}} \right)} \right] g \rho_r \delta A \quad (32)$$

It is clear that $\bar{\rho} - \rho_r \geq 0$ and equivalently $A_z \geq 0$ if θ and p are uncorrelated and if the p term is not more than 1/10 of the θ term.

If we assume $\theta' = kp'$, the condition for a positive integrand can be found from the solution of

$$1 - (5/49)k^2 - (5/7)k = 0$$

which gives

$$\bar{\rho} - \rho_r \geq 0 \quad \text{if} \quad -7.2 \lesssim k \lesssim 1.2$$

It is worth noting that A may be calculated to any desired degree of accuracy by adding more terms to (30) and using (32) and (28). In most applications, however, data will be available in isobaric coordinates (whose use includes the assumption of hydrostatic equilibrium) so that (32) becomes

$$A_p = \int g \rho_r \left(\frac{\theta'}{\theta} \right)^2 \delta A$$

and hence

$$A = - \int_{p(0)}^0 \overline{\left(\frac{\theta'}{\theta} \right)^2} z(p) dp$$

5. The Rate of Change of Available Potential Energy and Entropy

Since the publication of Lorenz' paper both theoretic and empirical studies have been made of how available potential energy is created and then used in the maintenance of the general circulation. To the extent that the atmosphere is a heat engine, we can expect that its ability to do work is controlled by entropy and that the approaches of Lettau and Lorenz have much in common.

It has been shown in the previous sections that available potential energy may be defined as the work done in increasing the entropy on every horizontal surface. This definition links the concept of available potential energy to the thermodynamic theorems involving the necessity of an entropy increase during the spontaneous flow of an unconstrained

system. This is, furthermore, the fundamental reason for available potential energy being non-negative.

We might expect that if the atmosphere were insulated from solar radiation and if outgoing radiation were stopped, that this state of maximum entropy might be reached after all of the available potential energy was used.

On the global scale, it is reasonable to assume that the atmosphere preserves its horizontal averages, so that the summer increase of the total potential energy and decrease of kinetic energy in one hemisphere is balanced by opposite effects in the other. If we thus take all time derivatives of horizontal averages as zero, (21) yields

$$\frac{dA}{dt} = \int \frac{\partial S}{\partial t} \left[\frac{g}{C_p} \frac{\partial p_r}{\partial z} / \left(\frac{\partial \theta}{\partial z} \right)^2 \right] \delta \tau \quad (34)$$

which shows that changes in available potential energy are a weighted average of local entropy changes.

Expansion of the substantial derivative of (4) and use of the hydrostatic assumption in the reference state produces the expression

$$\frac{dA}{dt} = - \int \left[\frac{T_r}{T} \frac{\partial q}{\partial t} + T_r \left(\frac{1}{T} \underline{v} \cdot \nabla q - \underline{v} \cdot \nabla S \right) + \frac{T_r}{T} \frac{\partial v_i}{\partial x_k} \Delta_{ik}(\mu) \right] \frac{(\gamma_h - \gamma_r)}{(\gamma_d - \gamma_r)^2} \gamma_d \rho_r \delta \tau \quad (35)$$

The first quantity in brackets is essentially what Lettau measured as a global average and found negative. The last term is the heat added by friction. Since both the heat energy and entropy gradients tend to be in the same direction and generally perpendicular to the wind, we may assume that the second term is small. In the summer hemisphere with

less pronounced differential heating, the first term may be of small magnitude and even positive, so that with the effects of friction, the available potential energy decreases. Conversely, in the winter hemisphere, we may expect, on the basis of Lettau's calculations, that the first term is strongly negative — enough, in fact, to more than balance the friction term — and thus provides an increase in the available potential energy.

Acknowledgments

The author is indebted for the advice, encouragement, and suggestions at various stages of this work offered by Professors R. A. Bryson, H. H. Lettau, L. H. Horn, and V. E. Suomi, and Mr. D. R. Johnson, all of the Department of Meteorology, University of Wisconsin.

The research reported here was partially supported by the U. S. Department of Commerce (Weather Bureau) with Contract Cwb 10240.

Table of Symbols

p	pressure
ρ	density
α	specific volume: $\alpha p = 1$
T	absolute temperature
θ	potential temperature: $\theta = T(1000/p)^{R/C_p}$
C_v	specific heat at constant volume
R	atmospheric gas constant
C_p	specific heat at constant pressure: $C_p = R + C_v$
$\frac{dq}{dt}$	rate of external heat addition per unit mass (in mechanical units)
S	entropy per unit mass (in mechanical units)
\mathcal{V}	wind vector
v_i	i th component of \mathcal{V}
$\Delta_{ik}(\mu)$	friction term: $\Delta_{ik}(\mu) = \mu \left\{ \frac{\partial v_i}{\partial x_k} + \frac{\partial v_k}{\partial x_i} - \frac{2}{3} \frac{\partial v_j}{\partial x_j} \right\}$
τ_{ij}	component of stress tensor: $\tau_{ij} = \mu \frac{\partial v_j}{\partial x_i}$
Π	total potential energy: $\Pi = \int (C_v T + gz) \rho \delta\tau$
K	total kinetic energy: $K = \int \rho \frac{V^2}{2} \delta\tau$
A	available potential energy
(λ, ϕ, z)	spherical coordinates: λ , longitude; ϕ , latitude; z , geopotential height above the earth's surface
a	the radius of the earth
g	the acceleration of gravity

- Z the "top" of the atmosphere
- γ lapse rate where $\gamma_d = g/C_p$ is the dry adiabatic lapse rate, $\gamma_h = g/R$ the autoconvective, and γ_r is the lapse rate of the reference state.

Mathematical Symbols

- $\int \{ \} \delta\tau$ integration over the entire atmosphere with respect to unit volume, $\delta\tau$
- $\int \{ \} \delta A$ integration over a geopotential surface with respect to unit area, δA
- \oint surface integration over bounding surface
- $\delta\tau$ unit volume: $\delta\tau = a^2 \delta A dz$
- δA unit area: $\delta A = \cos \phi \, d\phi \, d\lambda$
- $\frac{d}{dt}$ total derivative: $\frac{d}{dt} = \frac{\partial}{\partial t} + \mathbf{V} \cdot \nabla$
- $\frac{\partial}{\partial t}$ partial or local derivative with respect to time
- ∇ Hamiltonian operator
- \mathbf{N} unit exterior normal vector to bounding surface
- \ln natural logarithm
- f an arbitrary function
- Δz distance to reference position: $\Delta z = z_a - z_r$
- r denotes reference state
- ' denotes permutation from reference state: $f' = f - f_r$
- $\bar{(\)}$ horizontal average of ()
- ΔS entropy difference

References

- Lettau, H., 1954: A study of mass, momentum and energy budget of the atmosphere, Archiv f. Meteor., Geophy., u. Bioklimatologie, 7, 135-157.
- Lorenz, E. N., 1955: Available potential energy and the maintenance of the general circulation, Tellus, 7, 157-167.
- Margules, M., 1904: Über die energie der sturme, Jahrb. Zentr. Anst. Meteor., Vienna, 1-26 (Translation by C. Abbe in Smithson. Misc. Coll., 51, 1910).
- Spar, J., 1949: Energy changes in the mean atmosphere, J. of Meteor., 6, 411-415.
- Van Mieghem, J., 1956: The energy available in the atmosphere for conversion into kinetic energy, Beitr. z. Physik der Atmos., 29, 129-142.
- Van Mieghem, J., 1957: Energies potentielle et interne convertibles en énergie cinétique dans l'atmosphère, Beitr. z. Physik der Atmos., 30, 5-17.
- White, R. M., and B. Saltzman, 1956: On conversions between potential and kinetic energy in the atmosphere, Tellus, 6, 357-363.

A STUDY OF TERRESTRIAL RADIATION
MEASURED BY TIROS II

Elford G. Astling
and
Lyle H. Horn

Abstract. Mean meridional and latitudinal profiles of outgoing long-wave radiation as measured by TIROS II from 50°S to 50°N for 27 days during the period November 26, 1960, to January, 1961, were prepared and studied. High values of outgoing radiation were found over cloudless subtropical regions and low values over higher latitudes and over cloudy equatorial regions. The land areas in the summer hemisphere had higher values of outgoing radiation than land areas in the winter hemisphere. Over the oceanic areas the values were more uniform between the summer and winter hemispheres. By extrapolating the mean meridional profile of outgoing radiation to the poles, it was possible to compute an albedo of .38. A partitioning of the data revealed the effect of limb darkening and its apparent dependence on latitude.

ACKNOWLEDGEMENTS

The authors wish to express their appreciation to Professor V. E. Suomi, Mr. Donald Johnson, and Captain James Corcoran for their helpful suggestions.

We are grateful to Mr. Charles Hutchins for his help with the computer programming, to Mr. John Hayter for drafting the figures, to Misses Joan Erickson, Elizabeth Brandt, and Emmy Lou Groves for their help in compiling the data, and to the United States Weather Bureau for providing the radiation maps.

INTRODUCTION

One of the important problems of meteorology is to determine how differential cooling within the atmosphere contributes to the maintenance of the atmosphere's circulation. Using radiation data measured by artificial earth satellites, it is now possible to make an initial study of space and time variations of the long-wave radiation flux to space. Prior to the advent of the meteorological satellites, knowledge of outgoing terrestrial radiation was based primarily on theoretical considerations and indirect quantitative evaluations. Average seasonal and latitudinal values of long-wave radiation have been computed by Simpson (1929), Baur and Phillips (1934-1935), Lettau (1954), Houghton (1954), London (1957), Davis (1961), and others. Recently the possibility of estimating the atmospheric infrared cooling from satellite observations was discussed by Suomi (1958). An analysis of infrared radiation measurements made by Explorer VII has revealed large-scale radiation patterns which are related to large-scale weather systems (Suomi and Weinstein, 1961). Winston and Rao (1962) related large-scale temporal variations in long-wave radiation measured by TIROS II to temporal variations in kinetic energy and available potential energy.

In this study the space and time averages and variances of a 27 day sample of outgoing long-wave radiation at the top of the

atmosphere are presented and compared with the results of other investigations. Latitudinal and longitudinal averages of long-wave radiation loss to space over continental areas are compared with averages over oceanic areas. The significance of limb darkening and its effect on the mean values are also considered.

BASIC DATA

The data used in this study were extracted from 27 days of outgoing long-wave radiation measurements made by TIROS II for the period November 26, 1960, to January 6, 1961. The 27 individual dates may be found in Figure 7. Daily composite radiation maps for channel 4 of the five-channel scanning radiometer were prepared by the Meteorological Satellite Laboratory of the United States Weather Bureau. The channel 4 radiometer measured radiation in the 7.2 to 32.6 micron region. See TIROS II Radiation Data User's Manual (1961). With corrections made for the non-flatness response of the filters, the radiation data on the Mercator maps essentially represent the total radiation emitted from the earth-atmosphere system. The radiation maps, printed on a Mercator projection with a 1:20,000,000 scale, encompassed an area from 50°N to 50°S for all longitudes except for two regions — Central Asia, and the high latitude region of South America and the adjacent southeastern Pacific and southwestern Atlantic Oceans.

The five-channel scanning radiometer on TIROS II was shielded by a cone which permitted the sensor a 5° angle of view. When looking directly below, the cone subtended an area approximately 60 km in diameter. The radiometer had two views from the satellite. One view was through the floor of the satellite at an angle of 45° to the spin axis

and the other view was through the wall of the satellite in the opposite direction. Thus as the satellite rotated about its axis one field of view swept across the earth while the other view was directed to space. In a single sweep the sensor scanned the earth with angles of view ranging from glancing angles at the horizon to views directly below the satellite. From each sweep of the sensor a number of discrete radiation measurements were taken. In general, sweeps near the periphery produced fewer observations than those which covered areas near the subsatellite path. The discrete measurements within a given area, equivalent to $2\frac{1}{2}^\circ$ latitude square at the equator, were averaged and these values used in the preparation of the radiation maps.

With such a scanning device, observations made at different angles of view are not directly comparable. Radiation measurements obtained from areas near the horizon tend to be lower than measurements made directly below the satellite — i. e., limb darkening occurs. Thus an empirical correction factor developed by Wark et al. (1962) was employed in the preparation of the basic radiation maps. However, an examination of the maps revealed some elongated areas of higher radiation values along the orbital path, indicating that the limb darkening correction may not always have been sufficient. An analysis of the effect is included in this study.

In order to obtain a sufficient sample for the computations of longitudinal and latitudinal averages and variances, the data from the

subsattellite points were divided into two groups. One group was read at parallels ending in 0 and 5 degrees and a second group at meridians ending in 0 and 5 degrees. The groups consisted of 3,017 and 4,563 cases, respectively.

METHOD OF ANALYSIS

To eliminate the less reliable data obtained at large nadir angles (i. e., the angle between a line extending from the satellite to the subsatellite point on the earth and the line along the direction of view of the satellite's radiation sensor), values from the composite radiation maps initially were read at 5 degree latitude-longitude intersection from areas having 10 or more discrete measurements. Such areas always lie within regions delineated by nadir angles of less than 56° . From the 7,269 measurements obtained in reading the maps, averages were computed at 5 degree latitude intervals between 50°N and 50°S . These values together with the number of cases for each parallel are included as curve B in Figure 1.

It was noted that the latitudinal means computed from areas of 10 or more observations were lower than measurements obtained from balloon-borne radiometers (Sabatini, 1962) and the Explorer VII satellite (House, 1962). In an attempt to determine whether this difference could be attributed to an insufficient limb darkening correction in the TIROS II data, a second sample consisting only of data along the subsatellite path was used. Since the radiation maps were compiled from only single mode data, measurements along the subsatellite path

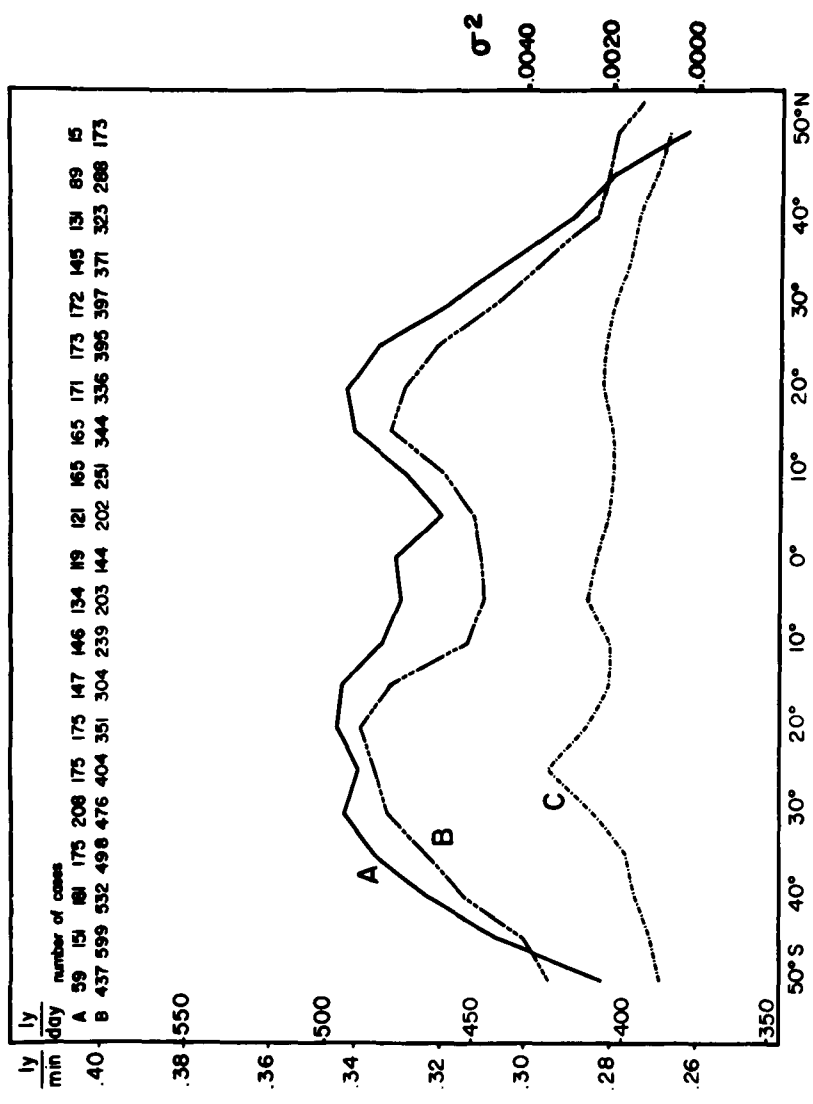


Figure 1. Average latitudinal values of outgoing long-wave (7-33 u) radiation from TIROS II for 27 days (Nov.1960-Jan.1961). Curve A, means computed from subsatellite data. Curve B, means computed from areas having more than 10 observations. Curve C, variances of subsatellite values.

were taken at angles less than 26° from the local vertical. See TIROS II Radiation Data User's Manual Supplement (1961). For angles of this order or less, Wark et al. (1962) have shown that the limb darkening effect is less than 1 per cent. However, even when only subsatellite data were used the TIROS II means were less than means computed from Explorer VII and TIROS III subsatellite data, indicating that calibration differences may be involved.

Calculation of means and variances for the subsatellite data were performed on an IBM 1620 computer. Latitudinal and longitudinal measurements of the outgoing terrestrial radiation were averaged to obtain mean radiation profiles. Variances of the radiative flux were computed with the intention of determining whether variations in the long-wave radiative cooling along parallels are as significant as along meridians. From an estimation of the outgoing radiation in high latitudes together with the satellite radiation measurements in the middle and low latitudes, the earth's albedo and zones of heat surplus and heat deficit were calculated. The subsatellite sample was also divided into land and oceanic cases to study the differences in the outgoing radiation over continents and oceans. Comparisons with theoretical studies and other observations were made to determine the accuracy of the results attained from the above procedures.

Because of the importance of understanding the time variation of outgoing long-wave radiation, computations of latitudinal means were

made for certain periods. To determine means for periods of more than a day, the data were divided into groups, each group representing consecutive days of radiation maps. Data not occurring on consecutive days were grouped with the closest period. No adjustments were made for the variations in areas sampled.

RESULTS

The results obtained from the 27 day sample are briefly presented below. Certain aspects of these results are discussed more fully in the next section where they are compared with the results obtained by other investigators.

Mean north-south profile. The mean outgoing long-wave radiation computed from the subsatellite data for parallels between 50° N and 50° S are plotted as curve A in Figure 1. This curve shows two zones of maximum outgoing radiation located in the Northern and Southern Hemispheric subtropics, respectively. Over the equatorial region, which separates these zones, the outgoing radiation is appreciably less. Radiation values greater than 480 ly day^{-1} were located between 10° and 35° S and between 15° and 25° N. The greater latitudinal extent of the zone of maximum outgoing long-wave radiation south of the equator is probably due to the greater solar heating in the summer hemisphere. The high values measured for the subtropical latitudes are the result of fewer clouds and lower water vapor content. In the equatorial regions where the surface temperatures are high and over 80 per cent of the surface is water, the relatively low values can be explained by the incident solar radiation involved in the evaporation-condensation cycle

and by the strong depletion of infrared cooling in the troposphere by extensive cirrus layers (London, 1957; Sabatini, 1962).

Limb darkening. The latitudinal averages of the radiation values from areas having 10 or more observations are presented as curve B in Figure 1. These lower values illustrate how limb darkening is affected by water vapor in the atmosphere. In general, the subsatellite means (curve A) are about 3 per cent higher than means computed from the data of 10 or more observations. However, between latitudes 5° N and 10° S the difference is more than 6 per cent, and poleward of 45° the subsatellite means are about 3 per cent lower, indicating that the limb darkening effect is dependent on latitude. In a study of limb darkening Wark et al. (1962) found that at large zenith angles, high humidity aloft was the greatest factor in decreasing the intensity of long-wave radiation from the earth. Thus, an estimation of the mean meridional profile of the distribution of water vapor can be determined indirectly from the comparison of curves A and B in Figure 1. The greater difference between the curves in the region 5° N to 10° S is an indication of higher humidity aloft in the equatorial zone. It is noted that this concentration of water vapor is displaced slightly poleward in the summer hemisphere. Other evidence of high water vapor content in the tropics from satellite data was found in a case study of radiation measurements in the 5.6 to 6.7 micron channel on TIROS III by Nordberg et al. (1961). A large increase in atmospheric water vapor was

measured when TIROS III passed from a dry subtropical region into the equatorial region over Africa.

Latitudes of heat balance and heat transport. The mean latitudinal averages presented by curve A can be used to obtain the latitude at which the mean incoming solar radiation is balanced by the mean outgoing radiation without knowing the incoming value. Houghton (1954) has shown that the latitude of heat balance is coincident with the latitude having the same value of outgoing radiation as the mean for the entire earth. Moreover, latitudes with averages higher than the global mean are zones of heat surplus and latitudes with averages lower than the global mean are zones of heat deficit. Because the TIROS II data extended from 50°S to 50°N, an extrapolation of the data to high latitudes was necessary in order to make such calculations. A description of the extrapolation method is included in the discussion of the albedo.

Using this approach, a global mean of $.311 \text{ ly min}^{-1}$ was estimated. From this value the latitude of heat balance in the winter hemisphere was found, from curve A in Figure 1, to be at 35° and in the summer hemisphere at 47°. An average of these two hemispheric values corresponds favorably with Houghton's value of 40° as the annual mean latitude of heat balance.

Land and ocean differences. When the radiation data were divided into two groups, one for observations over land and another for

observations over oceans, some interesting differences were found. The latitudinal means of outgoing long-wave radiation over land varied considerably, whereas the oceanic cases were more uniform. For both cases the radiation profiles are a reflection of the climatic patterns. The results are presented in Figures 2, 3 and 4.

The north-south profile (Figure 2) shows a low latitude region of minimum long-wave flux located between 5°N and 15°S for land cases and between 10° and 5°N for oceanic cases. Because of the relatively high surface temperatures in the equatorial regions, these lower radiation values must be attributed to the extensive cloudiness and high water vapor content of the atmosphere in this region. The cloudiness is likely associated with the intertropical convergence zone which assumes a more southerly position over the continents than over the oceans during the Southern Hemisphere's winter. The latitudes of minimum long-wave flux agree remarkably well with the mean position of the intertropical convergence zone for December as presented by Trewartha (1961). Over Africa the intertropical convergence zone migrates southward to about 15°S during the southern summer while in the eastern Pacific it is located about 50°N . These latitudinal differences of outgoing long-wave radiation are clearly reflected in the meridional profiles for land and oceanic areas.

Another difference in the outgoing long-wave radiation between land and ocean is noted in the subtropics. At these latitudes the long-wave

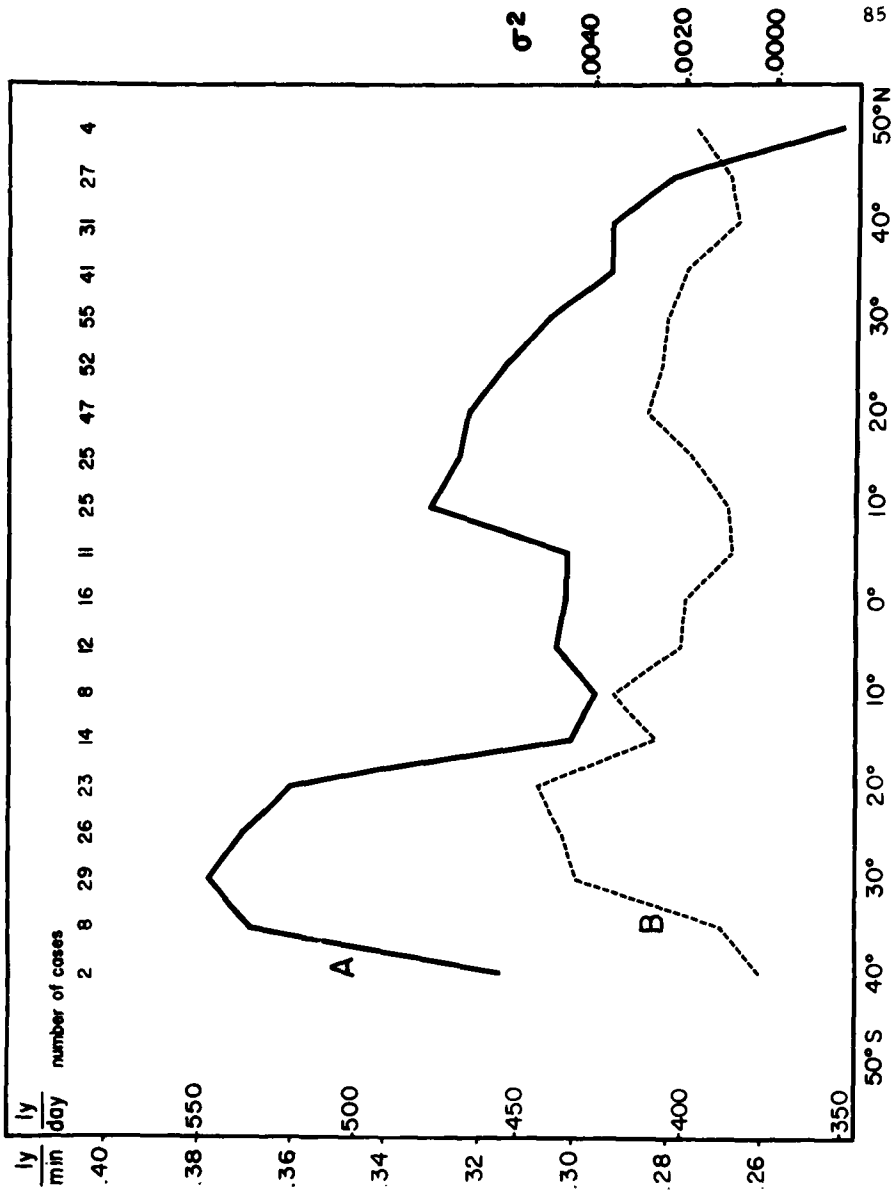


Figure 2. Average latitudinal values of outgoing long-wave radiation for land cases. Curve A, means. Curve B, variances.

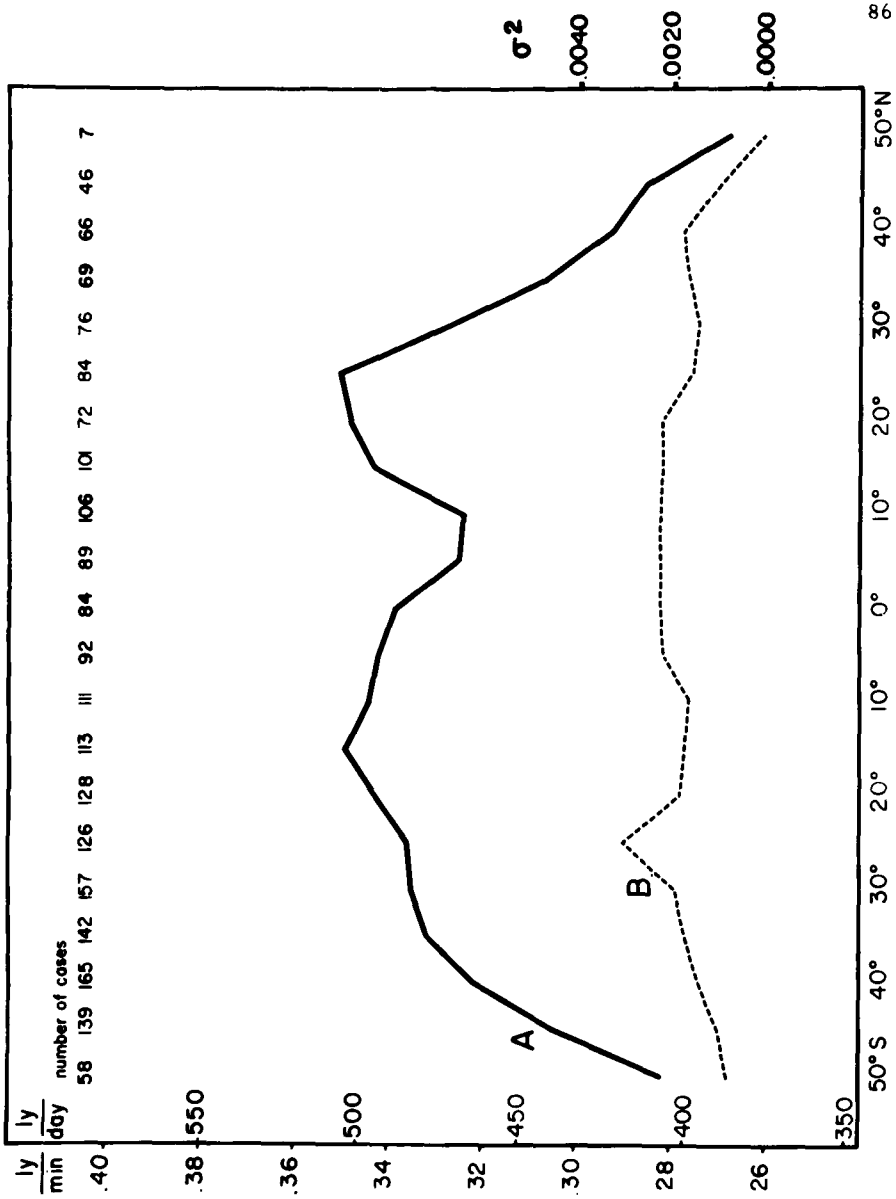


Figure 3. Average latitudinal values of outgoing long-wave radiation for oceanic cases. Curve A, means. Curve B, variances.

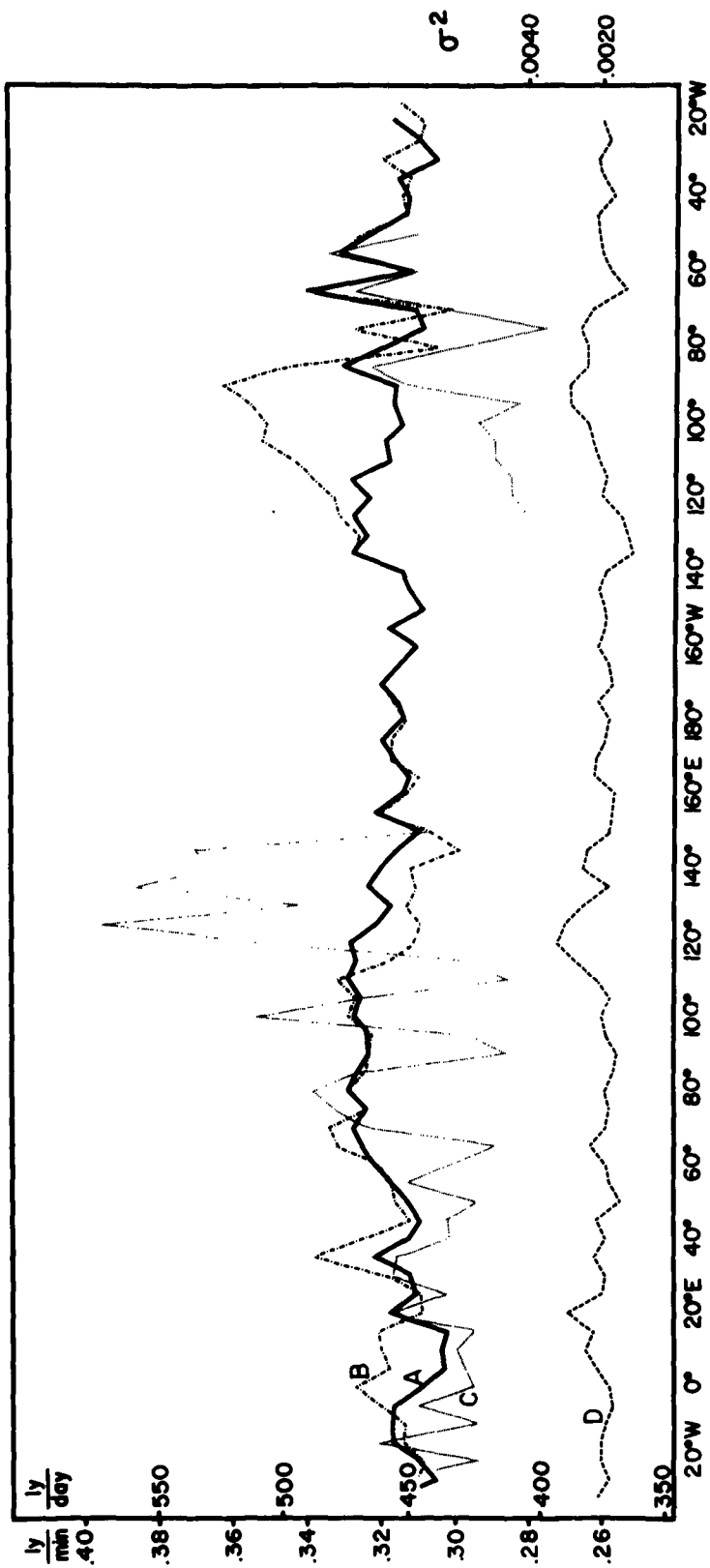


Figure 4. Average longitudinal values of outgoing long-wave radiation computed from subsatellite data. Curve A, averages for all cases.

Curve B, averages for oceanic cases. Curve C, averages for land cases. Curve D, variances of all cases.

radiation flux over the oceans reaches a value of about 500 ly day^{-1} in both hemispheres. On the other hand, the maximum values for subtropical land areas reach 540 ly day^{-1} in the summer hemisphere and only about 475 ly day^{-1} in the winter hemisphere. Since the subtropics of both hemispheres are relatively cloudless, the outgoing radiation of these areas is greatly influenced by the surface temperatures. The uniform flux from the oceanic areas of both hemispheres reflects the uniform ocean temperatures. However, the lower values over the land areas of the winter hemisphere compared with those of the summer hemisphere point up the stronger seasonal variations of land temperatures. It is also interesting to compare the latitudes of maximum flux for the land cases. In the summer hemisphere the maximum occurs at 30°S while in the winter hemisphere it occurs at 10°N . This latitudinal difference may be due to the southward extension of middle latitude cyclonic activity and associated cloudiness in the winter hemisphere. The gradual increase in long-wave flux from 35°N and 10°N seems to support this contention. One would expect the cloudiness associated with middle latitudinal cyclones to gradually decrease between 35°N and 10°N . A comparable latitudinal change in flux is displaced further south in the summer hemisphere.

Variations. The variances for the subsatellite data are shown as the dashed curve in Figures 1 to 4. The largest variances (i.e., values

greater than $.004 \text{ ly}^2 \text{ min}^{-2}$) occurred over the subtropical land masses of the summer hemisphere and the lowest variances occurred in the tropical land areas as shown in Figure 2. The large variances over the subtropical land areas were biased by daylight observations over Australia and thus may be the result of pronounced contrasts in outgoing long-wave radiation between the high surface temperatures of clear desert areas and the cold temperatures associated with high clouds. Evidently the low variances in the equatorial land region indicate a more uniform cloud cover over the region.

The meridional variances computed from the 50°N to 50°S latitudinal band are presented as curve D in Figure 4. It is noted that there are large variances centered around 20° and 120°W . The high radiation flux off the west coast of Central America and the low radiation flux at the same longitude to the north over the United States probably contribute to the large variance about the mean for the 120°W meridian. A similar situation exists at 20°W longitude, where an area of maximum radiation flux is present over the subtropical anticyclone in the South Atlantic Ocean and an area of minimum flux present over the intertropical convergence zone to the north over the African continent. This could explain the large variance at this longitude. In general, the variances in the long-wave radiation flux along meridians appear to be as large as along parallels.

Temporal variations. An idea of the temporal variation of the long-wave radiational cooling was obtained by computing short term latitudinal means of the subsatellite data, for four periods in which the land and ocean data were grouped. These means, plotted in Figure 5, show a decreasing rate of cooling at low latitudes from the first period, November 26 through 29, to the last period, December 28 through January 5. It is possible that these temporal variations are the result of a drift in the TIROS II calibration; however, since the temporal change in the long-wave radiation flux is much greater in low latitudes than in high latitudes, it seems unlikely that a calibration drift could alone account for the change. Thus it would appear that the latitudinal means of outgoing radiation experience significant short-term changes. It is possible that these low latitudinal variations of infrared cooling may be associated with the highly variable subtropical jet stream (Krishnamurti, 1961). In a similar study of outgoing long-wave radiation for latitudes between 20° and 55° N for practically the same period, Winston and Rao (1962) found an increase in available potential energy and an increase of kinetic energy at the lower latitudes. They suggested that the variations in outgoing long-wave radiation were probably related to a southward migration of the jet stream and associated high cloudiness during this period (Gelhard, 1961). The systematic temporal variations may also offer a clue as to a possible relationship between the general circulation of the Northern and Southern Hemispheres.

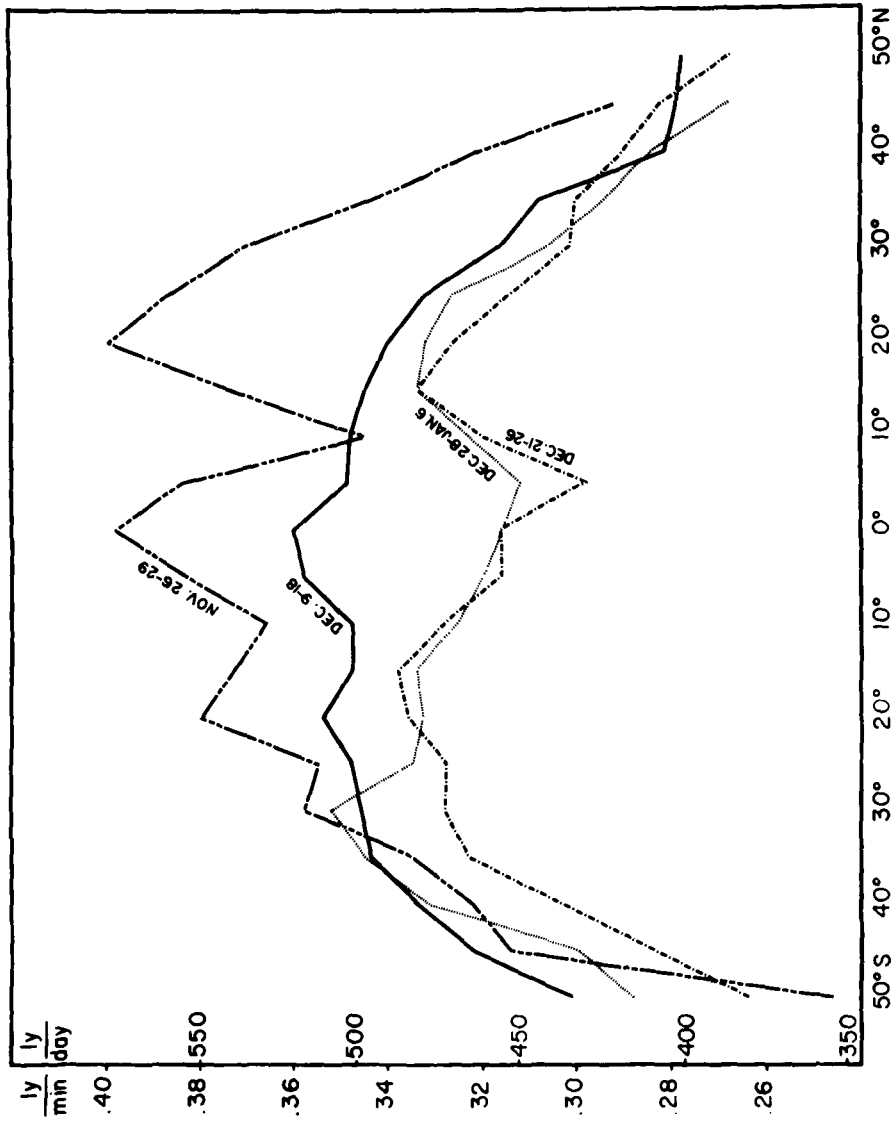


Figure 5. Average latitudinal values of outgoing long-wave radiation during four different periods.

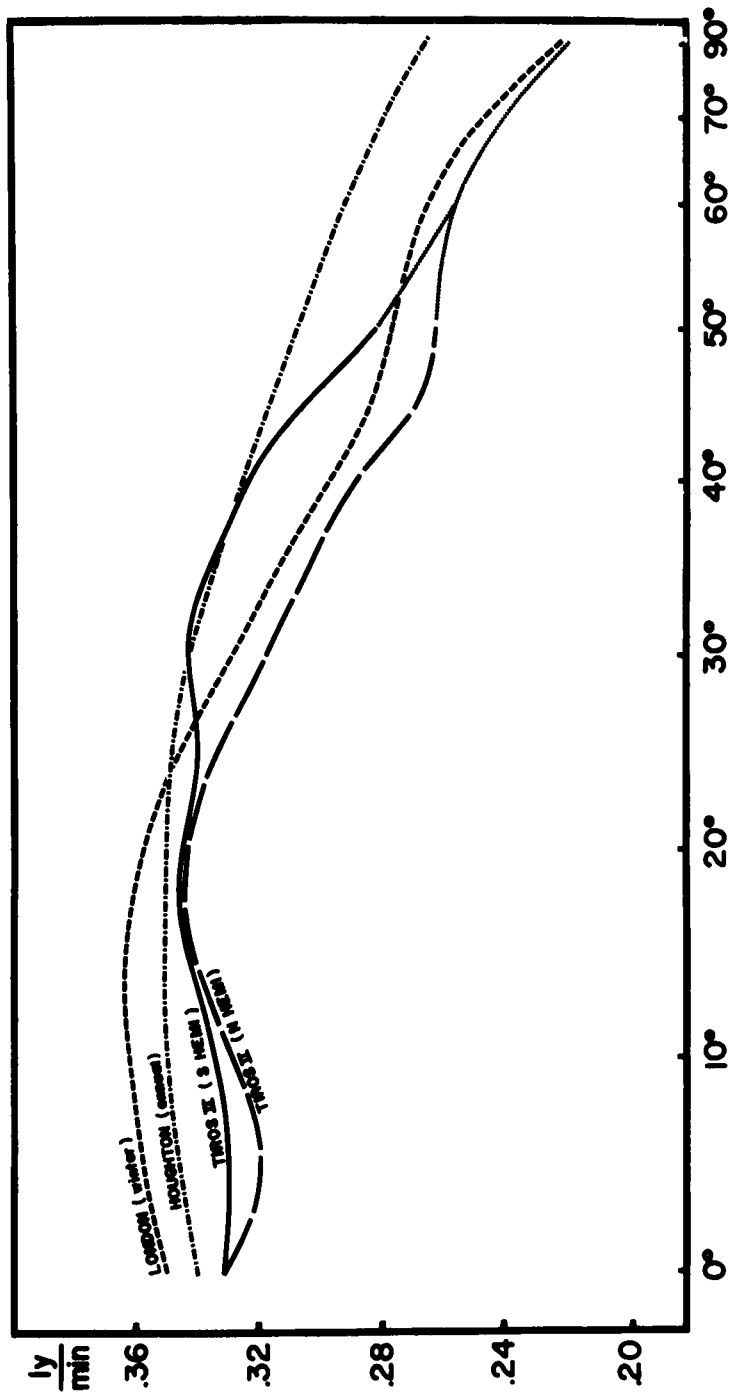


Figure 6. A comparison of average latitudinal values of outgoing long-wave radiation from TIROS II as a function of the sine of latitude with estimates from other studies.

COMPARISONS WITH OTHER STUDIES

Although the data sample used here was for only 27 days, the mean outgoing long-wave radiation computations compared favorably with those based on theoretical considerations. In a heat budget study for the Northern Hemisphere, London (1957) calculated latitudinal averages which were within 3 per cent of the averages calculated here. Houghton (1954), using mean soundings and the Elsasser chart, found 485 ly day^{-1} for the annual mean of outgoing radiation between 0° and 50° N which compares closely with the 465 ly day^{-1} obtained by averaging the Northern and Southern Hemispheric data from TIROS II. The comparison of the satellite data with London's and Houghton's results is shown in Figure 6. Other theoretical studies (Baur and Phillips, 1934-1935; Simpson, 1929) did not agree as closely. The estimation of the cloud amount appeared as the most important factor in the disparity of the outgoing radiation values.

The outgoing radiation measured by TIROS II was consistent with results obtained through other measurements. Data from radiometersonde flights made during the same time as TIROS II served as a valuable independent check (Sabatini, 1962). The average outgoing radiation at 30 mb from 170 wintertime radiometersonde ascents for seven stations over the United States was $.29 \text{ ly min}^{-1}$. Since the stratospheric

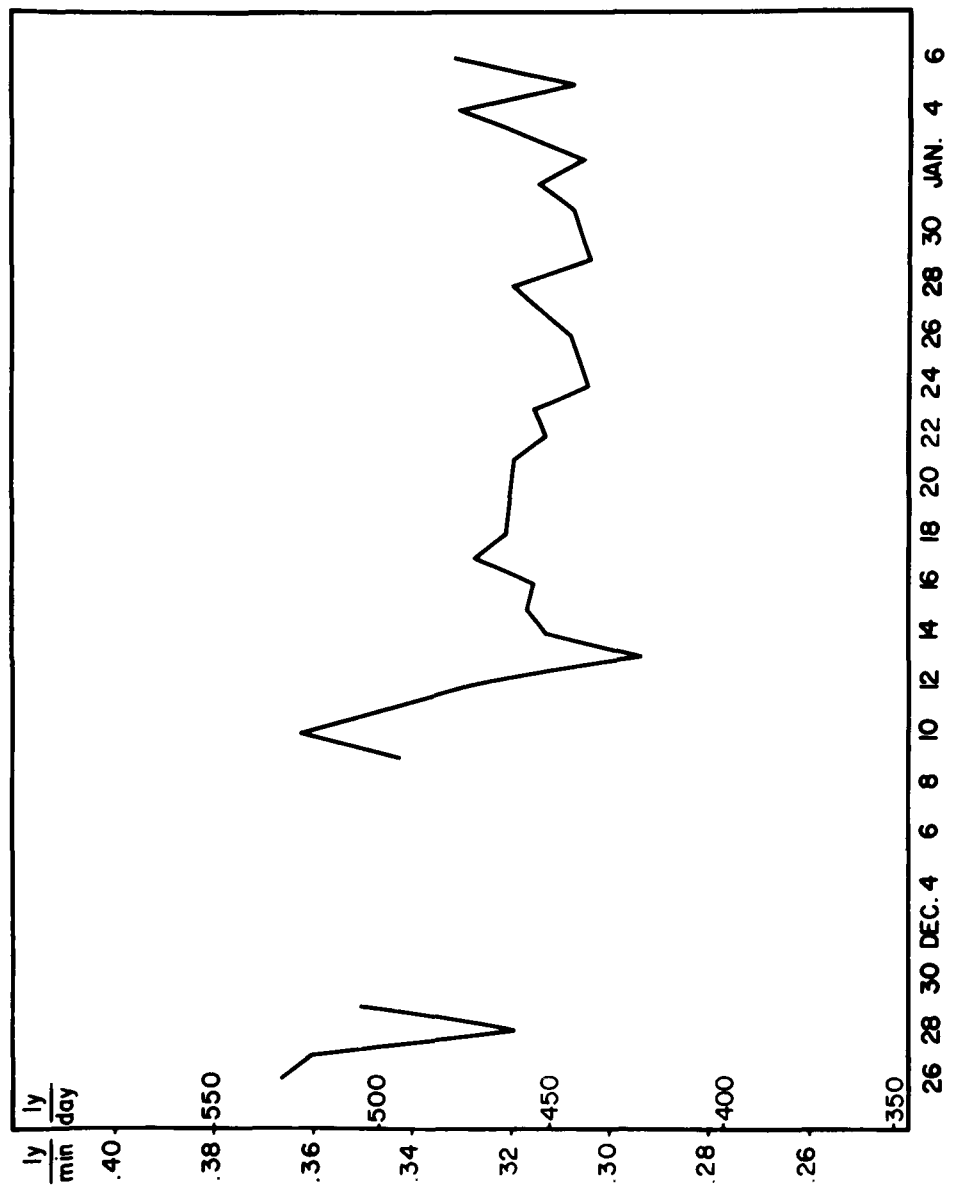


Figure 7. Daily means computed from subsatellite data.

temperatures above 30 mb are very low and there is less than 3 per cent of the atmosphere above this height, the outgoing radiation measured by the radiometersonde at 30 mb should be nearly equal to the radiation at the top of the atmosphere. The mean value from these stations, with an average latitude of about 40° N, was the same as that measured by TIROS II for 31 land cases along the 40° N latitude circle. Although encouraging, this excellent agreement may be in part fortuitous — especially since the data samples are relatively small.

A comparison of the albedo computed from the TIROS II data with other albedo estimates provided an interesting result. Using the Smithsonian Tables (1951) estimation of the solar constant as 2.01 ly min^{-1} for December, the amount of reflected radiation can be determined by finding the difference between incoming solar radiation and the outgoing terrestrial radiation. Since the radiation lost to space was known only for the latitudes between 50° N and 50° S, an estimation for the higher latitudes was necessary. These were calculated by extrapolating the means given by curves C and D in Figure 6 parallel to London's values (1957). The zonal averages of outgoing radiation are plotted against a sine function of latitude to represent a true area on the earth. A global average of $.311 \text{ ly min}^{-1}$ for outgoing radiation was then obtained from the mean value of the ordinates for the Northern and Southern Hemisphere. This value gave an albedo of .38 which is higher than the values of .34, which has been generally accepted by meteorologists, and .33 as

calculated from Explorer VII data for the 1959-1960 winter (House and Shen, 1962). It is possible that there is a considerable temporal variation in the albedo on a planetary scale. Nordberg et al. (1962) and Takasugi (1962) have found large variations of the albedo in preliminary studies of localized regions; however, more satellite observations will have to be made over extensive areas before any conclusion can be drawn.

SUMMARY AND CONCLUSIONS

From this study some interesting large-scale features of the outgoing radiation were found. The TIROS II data indicate an over-all cooling due to long-wave radiation lower than previous estimates; however, comparisons with Explorer VII and TIROS III radiation data suggest these low values may be the result of instrument calibration. In any event, the relative values of TIROS II seem quite good.

The consistency of the radiation data in presenting the effects of the geographical features suggests their value in obtaining a better understanding of the planetary controls of the general circulation. Future studies employing more extensive satellite data should provide a better estimation of the spatial and temporal variations of outgoing radiation.

BIBLIOGRAPHY

- Baur, F., and H. Phillips, 1934: Der Wärmehaushalt der Lufthülle der Nordhalbkugel. Beiträge zur Geophysik von Gerland, 42, 160-207; 1935, 45, 82-132.
- Davis, P. A., 1961: A Re-examination of the Heat Budget of the Atmosphere and Lower Troposphere. AF 19(604)-6146, Scientific Report No. 3, 115 pp.
- Gelhard, R., 1961: The Weather and Circulation of December 1960. Monthly Weather Review, 89, 109-114.
- Houghton, H. G., 1954: On the Annual Heat Balance of the Northern Hemisphere. Journal of Meteorology, 11, 1-9.
- House, F., 1962: Unpublished report, University of Wisconsin.
- Lettau, H., 1954: A Study of the Mass, Momentum, and Energy Budget of the Atmosphere. Archiv für Meteorologie, Geophysik und Bioklimatologie, Series A, 7: 133-157.
- List, R. J., 1951: Smithsonian Meteorological Tables, Sixth Edition, Washington, Smithsonian Institution.
- London, J., 1957: A Study of the Atmospheric Heat Balance. Final Report, Contract No. AF 19(122)-165, Department of Meteorology and Oceanography, New York University, 99 pp.
- Nordberg, W., W. R. Bandeen, B. J. Conrath, V. Kunde, and I. Persano, 1962: Preliminary Results of Radiation Measurements from TIROS III Meteorology. Journal of the Atmospheric Sciences, 19, 20-29.
- Sabatini, R. R., 1962: Wintertime Atmospheric Infrared Cooling over the Caribbean and the United States. Master's thesis, University of Wisconsin.
- Simpson, G. C., 1929: The Distribution of Terrestrial Radiation. Memoirs of the Royal Meteorological Society, 3, 53-78.

- Suomi, V. E. , 1958: The Radiation Balance of the Earth from a Satellite. Annals of the IGY, 6, 331-340.
- and R. R. Sabatini, 1962: On the Possibility of Atmospheric Infrared Cooling Estimates from Satellite Observations. Journal of the Atmospheric Sciences, 19, 349-350.
- Takasugi, S. , 1962: Methods of Albedo Determination from Explorer VII Satellite Radiation Data. Master's thesis, University of Wisconsin.
- TIROS II Radiation Data User's Manual, 1961: Goddard Space Flight Center, Greenbelt, Maryland, May 15.
- TIROS II Radiation Data User's Manual Supplement, 1962: Goddard Space Flight Center, Greenbelt, Maryland, May 15.
- Trewartha, G. T. , 1961: The Earth's Problem Climates. University of Wisconsin Press, Madison.
- Wark, D. G. , G. Tamamoto, and J. H. Liensch, 1962: Methods of Estimating Infrared Flux and Surface Temperature from Meteorological Satellites, Journal of the Atmospheric Sciences, 19, 369-384.
- Weinstein, M. , and V. E. Suomi, 1961: Analysis of Satellite Infrared Radiation Measurements on a Synoptic Scale. Monthly Weather Review, 89, 419-428.
- Winston, J. S., and K. Rao, 1962: Preliminary Study of Planetary-Scale Outgoing Long-Wave Radiation as Derived from TIROS II Measurements. Monthly Weather Review, 90, 307-310.

A STUDY OF THE MOVEMENT OF LONG ATMOSPHERIC WAVES

R. J. Deland

Abstract. The day to day changes of phase of the zonal Fourier harmonics of the 500 mb height are analyzed for six months of data. Since the phase changes are equivalent to movement of long waves, the wave speeds computed from the phase changes may be compared with the speed of Rossby waves of corresponding wave length. Good agreement is noted for wave numbers 4 to 10, while the long waves corresponding to wave numbers 1 through 3 remain quasi-stationary.

Introduction

Since Fourier harmonic expansions can be used to describe the large scale features of the atmosphere, an empirical study of the behavior of the individual harmonics is of interest. The main features of the day-to-day behavior of the zonal harmonics, obtained by Fourier analysis of the height of an isobaric surface around a latitude circle, have been described by Eliassen (1958). This paper consists of an analysis of the changes of phase-angle of the zonal harmonics. Since the longitudinal variation of isobaric height determines the meridional geostrophic wind component, the phase-angle of a particular zonal harmonic can be regarded as representing the longitudinal positions of the "waves in the westerlies" for the corresponding wave-length. The changes of phase-angle of the Fourier harmonics from day to day then represent the movement of the "waves in the westerlies."

The data used are the amplitudes and phase-angles for the Northern Hemisphere zonal harmonics computed by Horn (1961) for the 500 mb height on each day in the period October 1, 1951, to March 31, 1952. The height of the isobaric surface around the latitude circle is expressed as:

$$Z = \bar{Z} + \sum_{N=1}^{18} A_N \cos(N\lambda + \theta_N)$$

where Z is the height of the 500 mb surface (measured at 36 points around the latitude circle), \bar{Z} is the mean height of the 500 mb surface around a latitude circle, A_N is the amplitude of the N th harmonic, N is the wave-number, λ is the longitude, and θ_N is the phase-angle for the N th harmonic.

The phase difference of the N th harmonic between day, $j-1$, and day, j , is defined as

$$\Delta\theta_{N_j} = \theta_{N_{j-1}} - \theta_{N_j}$$

Thus, $\Delta\theta_{N_j}$ represents the movement of a particular "wave" during one day. The phase-difference was counted as positive (corresponding to progression) or negative (corresponding to retrogression) according to whichever sign was required to make the phase-difference numerically less than 180° . The ambiguities arising from this procedure when the displacements are large are discussed later.

Average Wave-Speeds

The average day-to-day phase difference for each of the months was determined for wave-numbers 1 to 10 for latitudes 40° , 50° , 60° N. The average phase differences were then divided by the wave-number. These results, which represent average daily speeds of propagation of the waves in degrees of longitude per day, are plotted as functions of wave-number in Figs. 1, 2, and 3. The average speeds for the whole six-month period are also shown in the same figures.

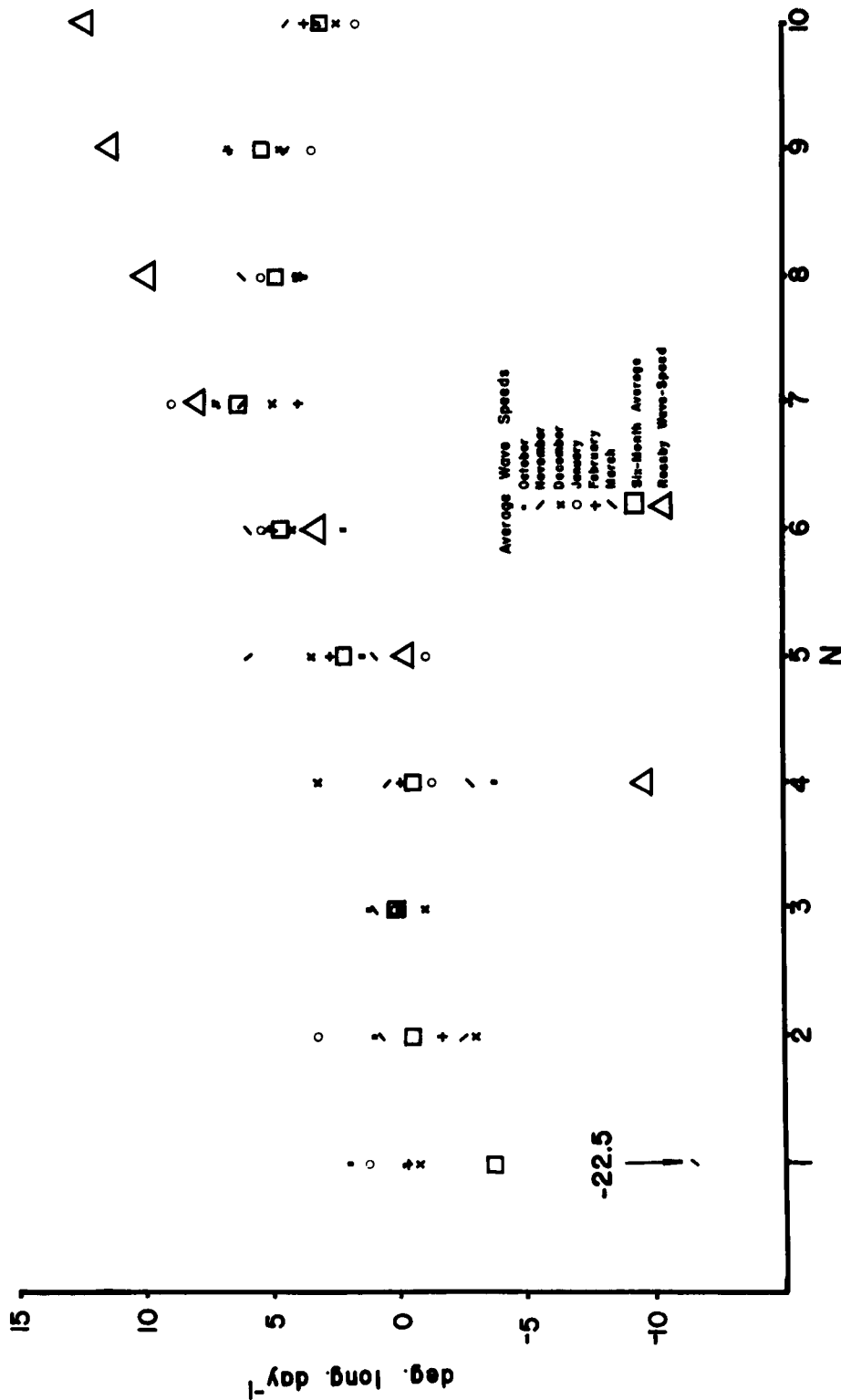


Figure 1. Mean and Rossby wave-speeds for wave-numbers 1-10, at latitude 40° N.

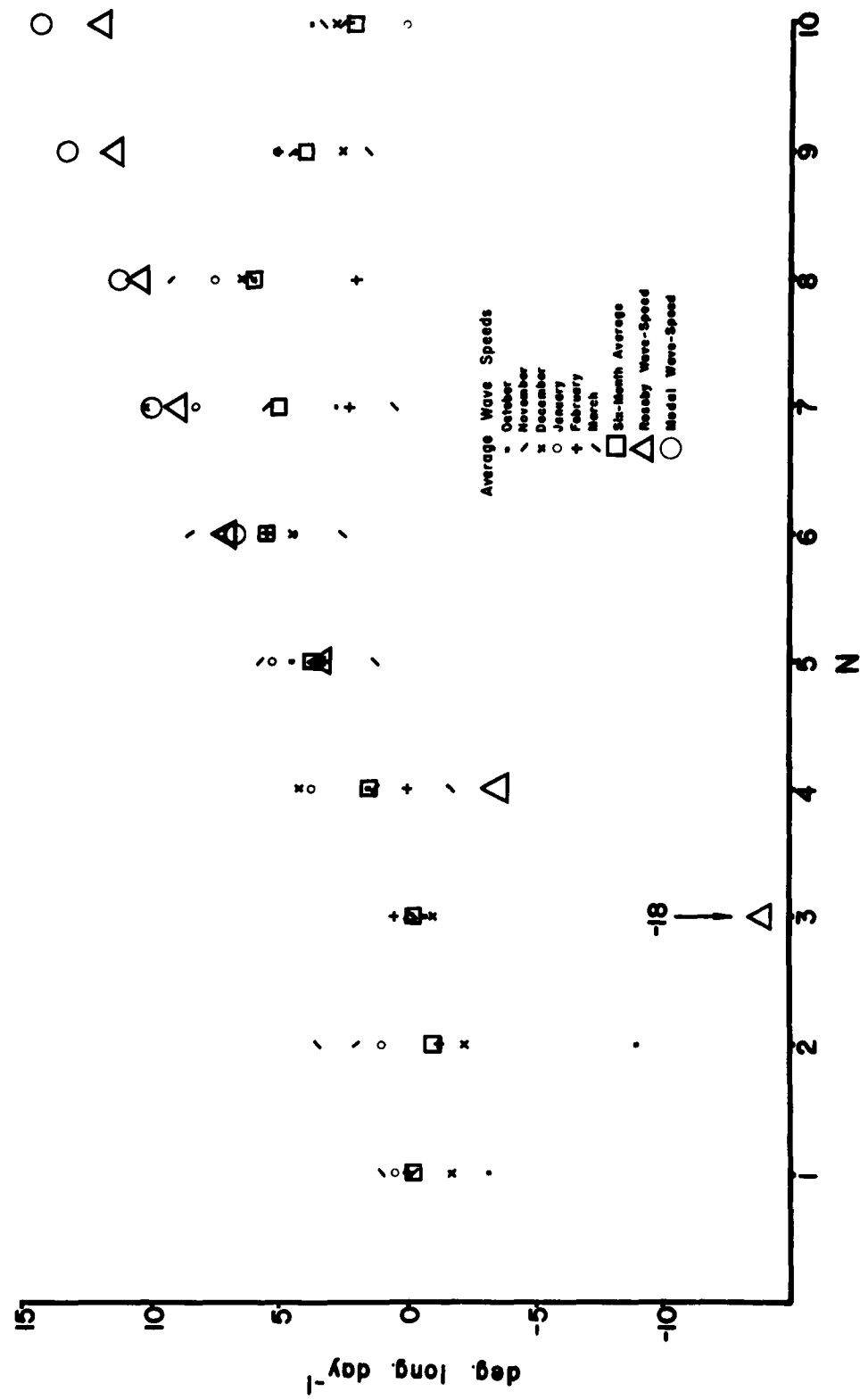


Figure 2. Mean, modal, and Rossby wave-speeds for wave-numbers 1-10, at latitude 50°N.

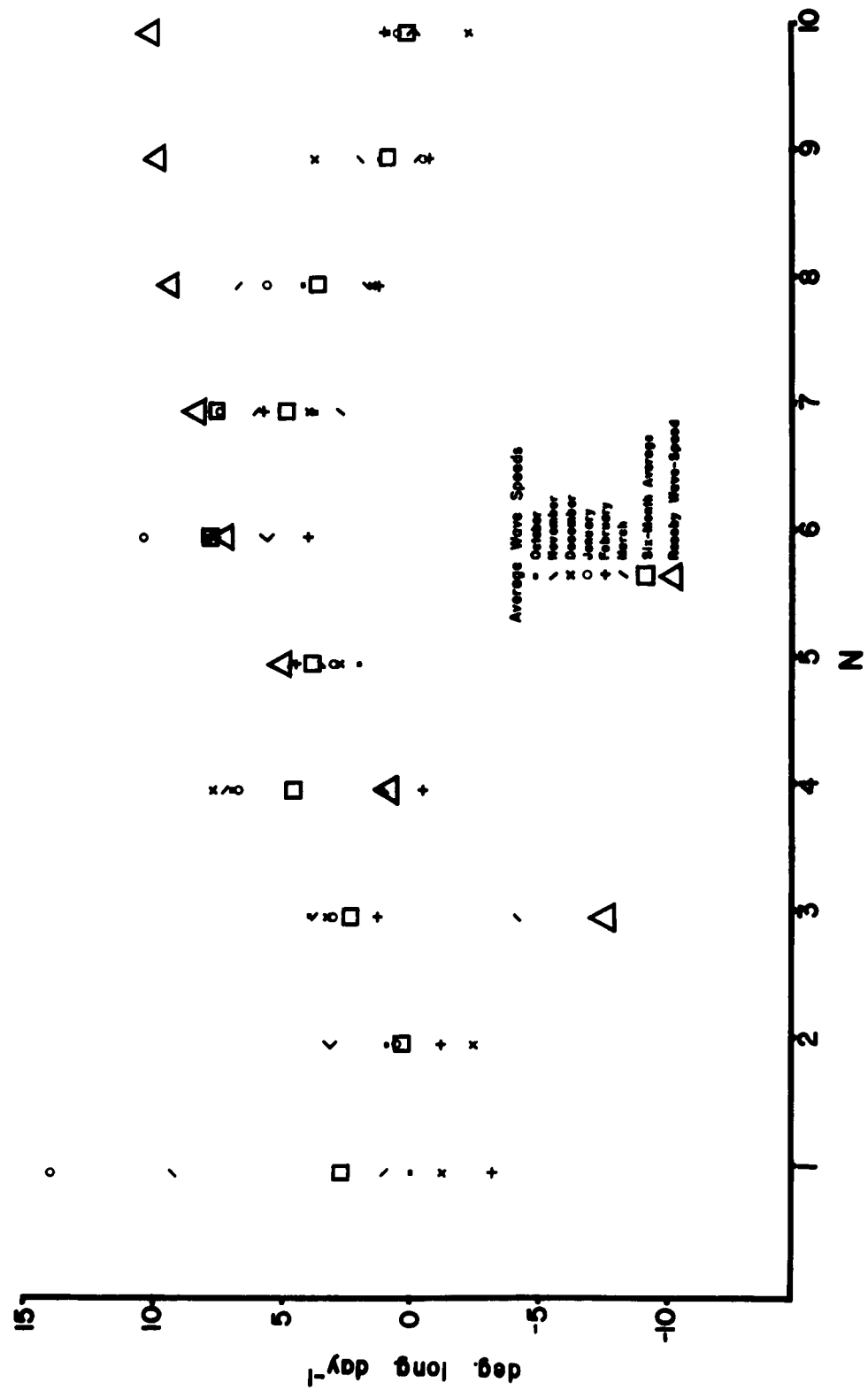


Figure 3. Mean and Rossby wave-speeds for wave-numbers 1-10, at latitude 60° N.

Only wave-numbers up to $N = 10$ are considered, for inspection indicates that the phases for higher wave-numbers are essentially random.

As would be expected, the six-month averages show that the longest waves ($N \leq 3$) are approximately stationary. However, the individual monthly averages indicate large and erratic speeds, apparently because the day-to-day phase differences (not shown) are sometimes large and random when the amplitude is small.

The shorter waves ($N \geq 5$) show progressive speeds. These wave speeds were compared with those calculated using the Rossby wave-speed formula,

$$C_R = U - \beta L^2 / 4\pi^2$$

where C_R is wave speed, U is the mean zonal wind speed, L is wave length, and β is the rate of change of the Coriolis parameter with latitude. U was calculated from the average six-month height difference across twenty degrees latitude. The calculated values of C_R are shown in Figs. 1, 2, and 3.

The quasi-stationary waves appear to be those for which the Rossby wave-speed is negative. The speeds of the traveling waves agree fairly well with the corresponding Rossby wave-speeds in the middle range of wave-numbers ($N = 4$ to 7). Above $N = 7$ the observed wave-speed drops off with increasing wave-number, being considerably less than the Rossby wave-speed for the highest wave-numbers considered here.

The wave-number separating traveling from quasi-stationary waves shifts from about 5 at 40°N to 3 or less at 60°N.

Examination of the individual day-to-day phase-differences for the higher wave-numbers show frequent alternations between numerically large (nearly 180°) positive and negative values. It appears probable that there are wave-movements of more than a half-wave-length, which were taken as negative differences in the original determination of the phase differences, thus reducing the average speed. This ambiguity of the wave-movements for the higher wave-numbers was mentioned by Eliassen (1958).

In an attempt to remove the ambiguity from the large displacements, a frequency analysis of the phase differences was made for wave-numbers 6 to 10 at latitudes 50°N. The possible values of the phase-difference, from -180.0° to +180.0°, were divided into thirty-six 10-degree classes (i. e., -179.9° to -170.0°, -169.9° to -160.0°, etc.). The number of occurrences, in the six-month period, of phase differences falling within each of the 36 classes was counted. Bar diagrams of the frequency distributions were then constructed by representing the number of occurrences as the ordinate and the phase-difference as the abscissa. The results are shown in Figs. 4 through 8. The distributions are continued beyond 180° as if the large negative differences represent positive differences greater than 180°.

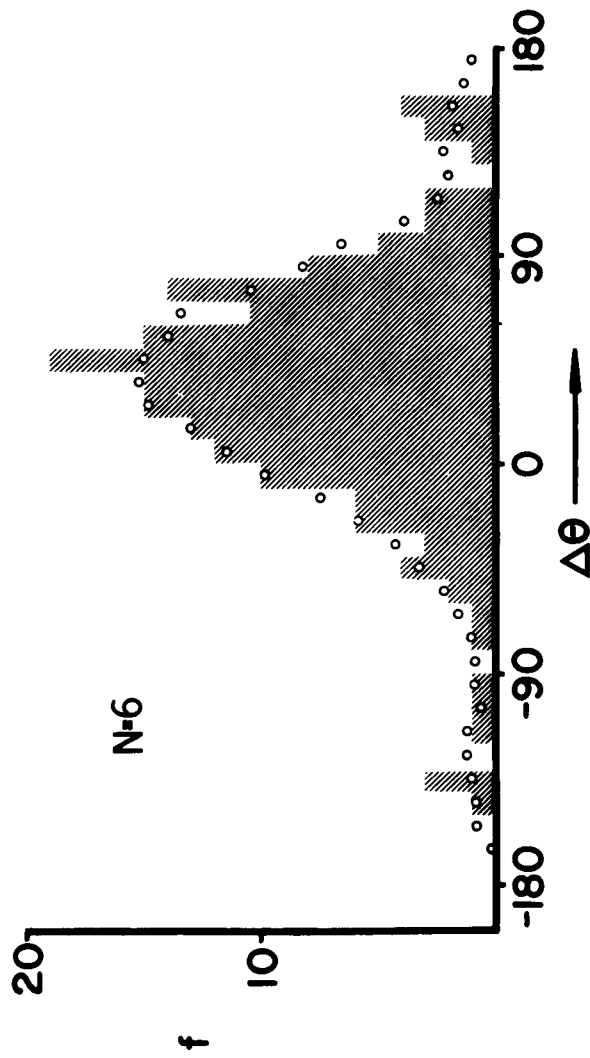


Figure 4. Frequency, f , of the day-to-day phase differences. Circles represent running means over five consecutive values of f . Wave-no. 6.

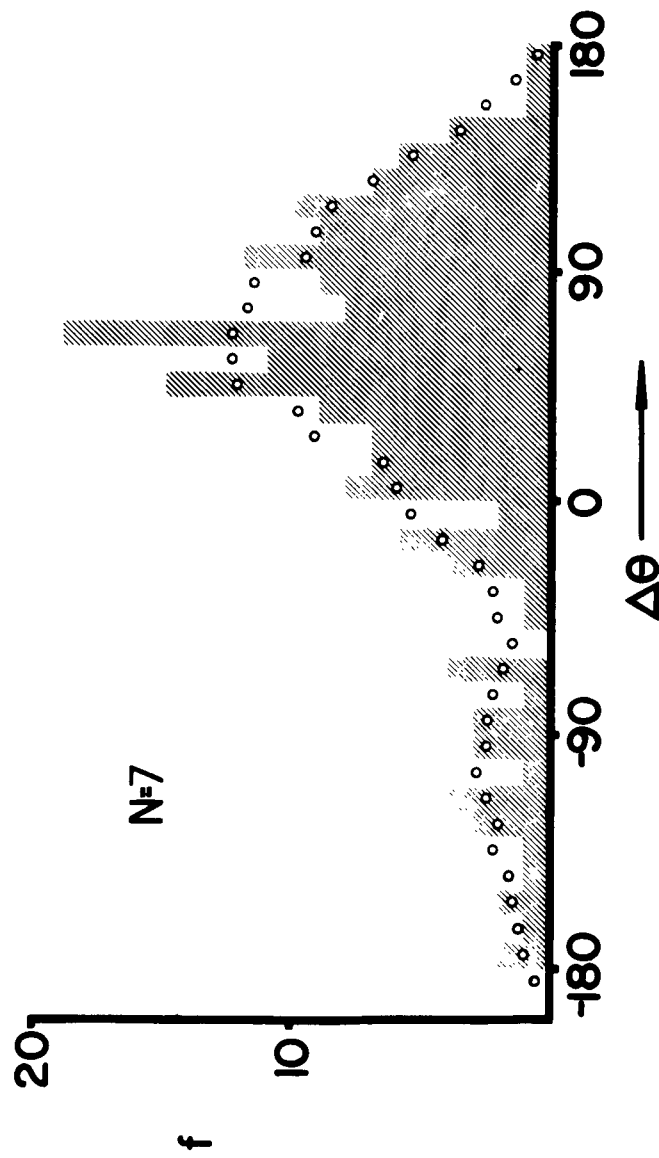


Figure 5. Frequency, f , of the day-to-day phase differences. Circles represent running means over five consecutive values of f . Wave-no. 7.

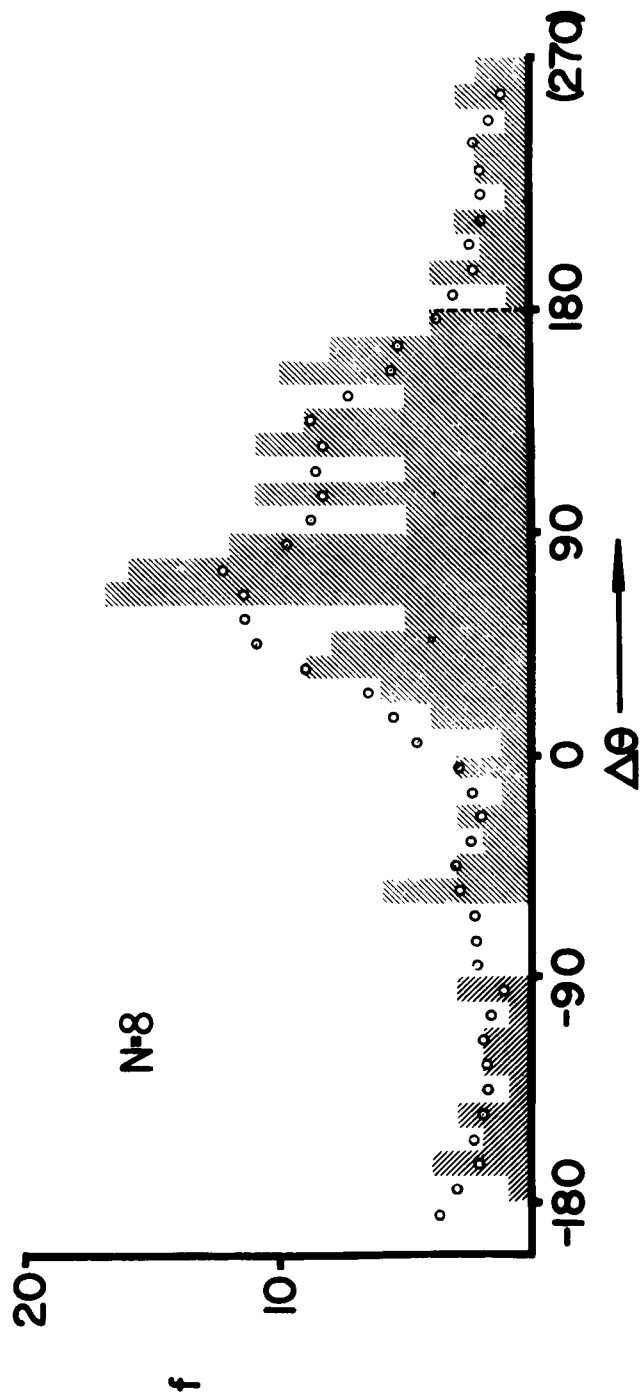


Figure 6. Frequency, f , of the day-to-day phase differences. Circles represent running means over five consecutive values of f . Wave-no. 8.

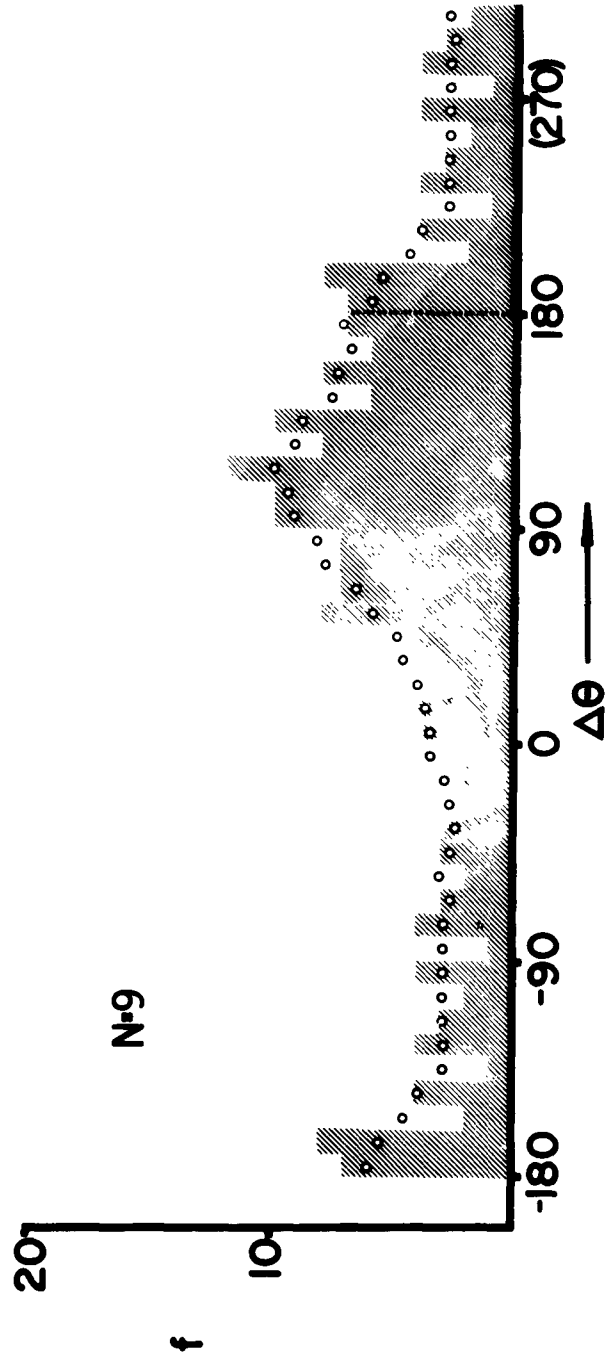


Figure 7. Frequency, f , of the day-to-day phase differences. Circles represent running means over five consecutive values of f . Wave-no. 9.

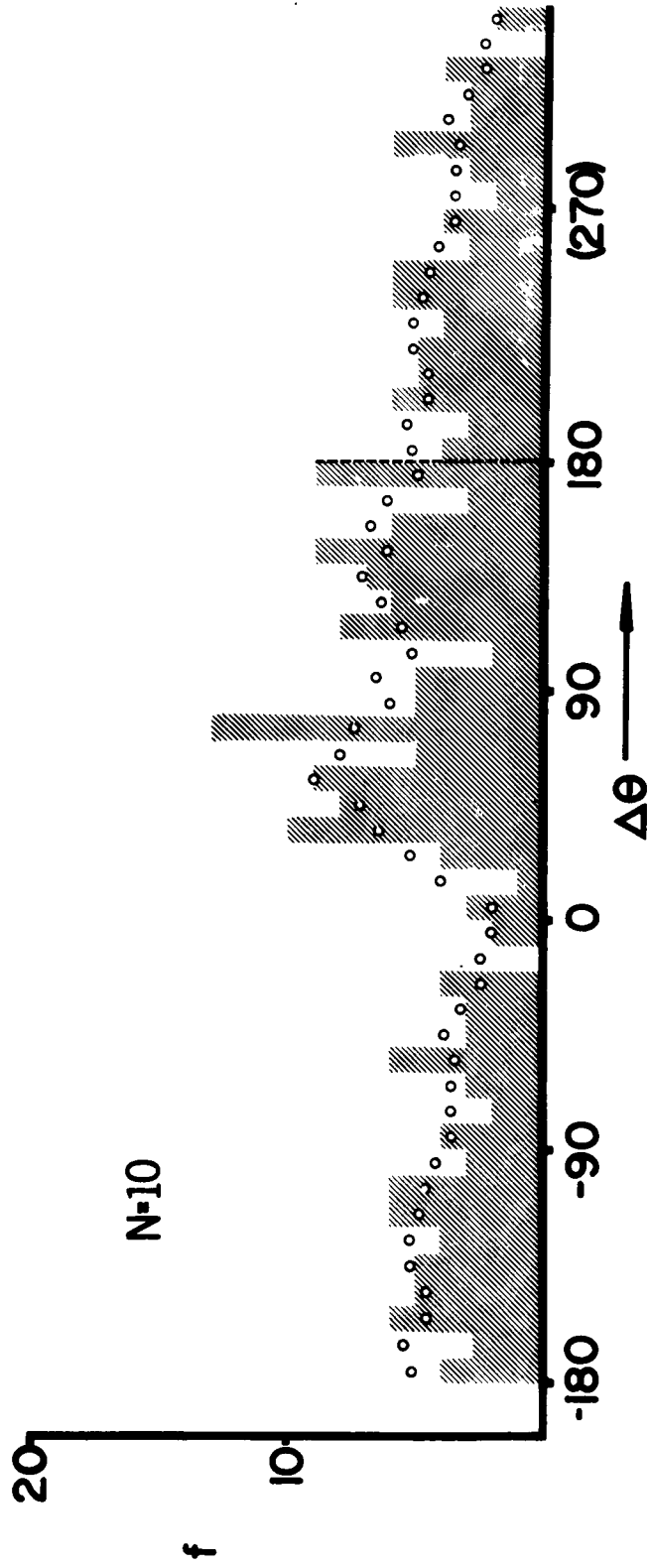


Figure 8. Frequency, f , of the day-to-day phase differences. Circles represent running means over five consecutive values of f . Wave-no. 10.

Because the discrete frequencies fluctuate considerably, the distributions were smoothed by plotting for each class interval the average of the frequencies for the five classes (corresponding to a phase difference range of 50°) centered on that class. In order to smooth the distributions near 180° they were assumed to be extended as described above. The symmetry of the distributions which results when they are extended supports the assumption made in extending them. It also suggests a model for the distribution of wave-speeds. If we assume that the true distribution is normal and that the noise resulting from random phases associated with small amplitudes is uniformly distributed, then the mode of the distribution is the best estimate of the wave speed. Since the original frequency distributions are erratic, the modes of the smoothed distributions were used to obtain the wave speeds. They are plotted in Fig. 2. For wave-number 10 the secondary rather than the primary mode of the rather asymmetrical distribution was chosen, since the secondary mode fits the general shape of the distribution better than the primary mode. The estimates of the wave-speed obtained in this way appear quite reliable except possibly in the case of wave-number 10.

The wave-speeds estimated from the frequency distributions agree well with the Rossby wave-speeds. The latter are, therefore, consistent with the observed speeds over the whole range of wave-numbers up to $N = 10$, except for the quasi-stationary waves with $N \leq 3$.

Acknowledgements

The author wishes to thank Mr. Jack Hayter for assistance in drafting the figures and Mr. Martin P. Sponholz for assistance in the computations.

Bibliography

- Eliassen, E. 1958. A study of the long atmospheric waves on the basis of zonal harmonic analysis. Tellus 10, 206-215.
- Horn, L. H. 1961. A statistical analysis of the relationship between the kinetic energy and potential energy of the atmosphere. Ph.D. Thesis, University of Wisconsin.